Dividend Suspensions and Cash Flows During the Covid-19 Pandemic: A Dynamic Econometric Model*

Davide Pettenuzzo† Brandeis University

Riccardo Sabbatucci‡ Stockholm School of Economics

Allan Timmermann§ UC San Diego

Abstract

Firms suspended dividend payments in unprecedented numbers in response to the outbreak of the Covid-19 pandemic. We develop a multivariate dynamic econometric model that allows dividend suspensions to affect the conditional mean, volatility, and jump probability of growth in daily industry-level dividends and demonstrate how the parameters of this model can be estimated using Bayesian Gibbs sampling methods. We find considerable heterogeneity across industries in the dynamics of daily dividend growth and the impact of dividend suspensions.

Keywords: COVID-19; high-frequency cash flows; dividend suspensions; predictive density modeling, Bayesian estimation

*We are grateful to two anonymous referees, an Associate Editor and Torben Andersen for comments on the paper. We also thank Ralph S.J. Koijen, Peter Phillips, Jun Tu, and Jun Yu for valuable suggestions on our paper. Finally, we received helpful comments from seminar participants at the Board of the Federal Reserve, Singapore Management University, UCSD, University of Nottingham, Queen Mary University and in the IAAE webinar series. We are grateful to Youssef Aljabi and Mark McAvoy for excellent research assistance.

†International Business School, Brandeis University. 415 South Street, MS 032 Waltham, MA 02453, USA. **Email:** dpettenu@brandeis.edu

‡Department of Finance, Stockholm School of Economics and Swedish House of Finance (SHoF). Sveavägen 65, 113 83 Stockholm, Sweden. **Email:** riccardo.sabbatucci@hhs.se

§Corresponding author. Rady School of Management, UCSD. 9500 Gilman Drive, La Jolla CA 92093-0553, USA. **Email:** atimmermann@ucsd.edu

1 Introduction

The outbreak of the Covid-19 pandemic, resulting lockdowns and stay-at-home orders had a sharp and unprecedented effect on economic activity and caused turmoil in global financial markets. Uncertainties about the future trajectory of the virus, policy responses of governments and central bankers, and shifts in household and firm behavior massively increased firms' cash flow risks.[1] Faced with extreme levels of uncertainty and sharp reductions in cash flows, many firms suspended dividend payments. Dividend policies reflect firms' expectations of future earnings, so their decision to entirely suspend dividends was a harbinger of the extreme slowdown in many sectors' economic activity that was to come.

Periods with extreme financial stress such as the Covid pandemic offer unique insights into what drives asset prices. Since the seminal work of Clark (1973), researchers have modeled the dynamics in return volatility under the assumption that the news clock can run at different speed . However, little is known about whether the extremely high levels of volatility in stock returns observed during periods of financial distress is driven by a similar volatility clustering in news about the underlying fundamentals.

A key challenge lies in measuring and quantifying the fundamentals news process at a relatively high frequency such as daily. One approach is to use textual analysis to count news stories. This approach, while promising, has the limitation that individual news stories are not equally important for economic fundamentals and so it is unclear how to map news counts to revisions in investors' views on fundamentals. Another approach, which we promote in this paper, is to collect high-frequency data on fundamentals such as dividends or earnings and model the dynamics in the resulting data. The chief challenge posed for this approach is the irregular arrivals process for news on (daily) firm-level dividends and the extreme heterogeneity in disaggregate dividend growth which tends to be dominated by large outliers.

We argue that such challenges require modeling three components in daily dividend growth data, namely a persistent mean process, a jump component that accounts for

[1] Studies on the effect of the pandemic on growth prospects and economic uncertainty include Gourinchas (2020), Eichenbaum et al. (2020), Atkeson (2020), and Ludvigson et al. (2020).

composition shifts and idiosyncratic firm news, and a stochastic volatility process. Generalizing the approach in Pettenuzzo et al. (2020), in this paper we develop a flexible multivariate econometric model that captures the highly irregular dynamics in daily dividends during the Covid pandemic and quantifies the effect of dividend suspensions on the distribution of dividend growth across five industries. We demonstrate that the signal value in dividend suspensions is very important and show that the proportion of dividend suspenders has a significant effect on the expected growth in dividends, its conditional volatility, and on the probability of jumps (outliers) in daily dividend growth. We also show that these effects display considerable heterogeneity across industries. Effects tend to be strongest for consumer goods and manufacturing stocks and weaker for stocks in the high tech and healthcare businesses.

Our paper is organized as follows. Section 2 introduces the data, including evidence on dividend suspensions during the pandemic. Section 3 explains our multivariate dynamic econometric modeling approach and describes our MCMC sampler. Section 4 reports empirical results, including parameter estimates for the multivariate model fitted to dividend growth dynamics across five industries. Section 5 concludes.

2 Data

This section introduces our data sources and provides evidence on how firms changed their dividend payment policies in response to the outbreak of the Covid-19 pandemic.

2.1 Dividend Suspensions

We begin our analysis by outlining how we collect data on daily dividend announcements, including those made by firms that suspended dividends, merging data from several sources.[2] To conduct comparisons with events during the Global Financial crisis (GFC), we use data going back to January 2005, starting a little less than three years prior to the GFC to enable us to assess this episode in a historical perspective.

[2]The stock market reacts to information in dividend announcements rather than to dividend payments which generally lag announcements by several weeks.

For the pre-Covid period from January 2005 through December 2019, we use data from the Center for Research in Security Prices (CRSP) to extract daily stock prices, shares outstanding, and dividend announcements for individual firms. Our data includes all ordinary cash dividends declared by US firms with common stocks (share codes 10 and 11) listed on the NYSE, NASDAQ, or AMEX exchanges.[3] To be included, we require firms to have valid stock prices and shares outstanding when dividends are announced. For the more recent period spanning January 1st through September 30th, 2020 we supplement the CRSP data with stock prices and dividend announcements collected from Bloomberg.

We obtain information on dividend suspensions from three other data sources. First, we use Capital IQ to extract dividend suspensions and cancellations of U.S. firms. However, this list is incomplete and often misreports the *actual* announcement date of the suspension. For each of the public companies included in our data set from CRSP, we therefore use the EDGAR database to download all 8-K forms that companies filed to the SEC between January 2005 and September 2020. 8-K filings are triggered by the arrival of information deemed to be "materially important" to firms' financial situation. We complement the information extracted from EDGAR by using the NASDAQ news platform to download recent press releases on companies in our sample.

Combining the textual data from EDGAR and the NASDAQ news platform, we identify the 8-K filings and press releases that mention dividend suspensions in either the text or in the title and extract the date of the suspension and the associated ticker using an automated text scraper. After manually reviewing each case to remove false positives, and cross-checking with Google and Bloomberg, we identify a total of 198 dividend suspenders in 2020 and 472 since 2005. Finally, we merge these suspensions with price and accounting data from CRSP/COMPUSTAT and Bloomberg.

For each day during the period January-September 2020, Figure 1 shows both the absolute number of firms suspending dividends (top panel) and the proportion of firms suspending dividends relative to all firms announcing dividend news (bottom panel). Dividend suspensions were rare in January and February, averaging less than one per week. The outbreak of the pandemic triggered a virtual avalanche of suspensions with

[3]Ordinary cash dividends have CRSP distribution codes below 2000.

some days seeing 100% of announcing firms suspending dividends and the suspension rate regularly exceeding 20% on a daily basis between mid-March and early April.

Figure 1 shows that large numbers of individual firms suspended their dividend payments literally within days of the pandemic outbreak and demonstrate how unusual such suspensions were prior to the March 11, 2020 WHO declaration of a global pandemic. The speed with which firms suspended dividends after the outbreak of the Covid-19 pandemic was historically unprecedented even compared against the GFC.

2.2 Daily Dividend Growth

We next describe how we construct a daily dividend growth measure that allows us to quantify the effect of dividend suspensions on the predictive distribution of future dividend growth. Our analysis closely follows Pettenuzzo et al. (2020) and computes dividend growth by comparing same-firm, same- (fiscal) quarter, year-over-year changes in cash flows, accounting for both firm-level heterogeneity and seasonal (quarterly) variation in dividend payments.

Let D_t^j denote the total dividends declared by firm j on day t, calculated as the dollar value of the dividend per share times the number of shares outstanding for firm j on day t. Next, let I_t^j be an indicator variable that equals one if company j announces quarterly dividends on day t–including an announcement of a dividend suspension–and otherwise is zero. Also, let $\tilde{t}_j^-(t)$ be the same-quarter, prior-year dividend announcement date for firm j. Aggregating across firms, the total dollar value of dividends declared on day t is $\sum_{j=1}^{N_t} I_t^j D_t^j$, where N_t is the number of publicly traded firms in existence on day t. Similarly, the total dollar value of dividends declared by the *same* set of firms for the *same* fiscal quarter during the prior year is given by $\sum_{j=1}^{N_t} I_{\tilde{t}}^j D_{\tilde{t}_j^-(t)}^j$.

From the ratio of these two numbers we can compute a daily measure of the aggregate, year-over-year (gross) growth in dividends, G_t:

$$G_t = \frac{\sum_{j=1}^{N_t} I_t^j D_t^j}{\sum_{j=1}^{N_t} I_{\tilde{t}_j}^j D_{\tilde{t}_j^-(t)}^j}. \tag{1}$$

Only firms for which $I_t^j = I_{\tilde{t}_j^-}^j = 1$ are included in this calculation, thus ensuring that the *same* firms are used in both the numerator and denominator of the ratio.[4]

Our dividend growth measure in (1) includes information on dividend suspenders in the following way: when a firm announces that it will not distribute a dividend in a given quarter, the numerator on that day for the firm in (1) will be zero, while the denominator will be the dividend announced for the corresponding quarter of the previous year, regardless of whether the firm paid dividends during that quarter.[5]

The two panels in Figure 2 show the distribution of dividend announcements and the resulting nominal amount of dividends announced by those firms between January 1st and September 30th of 2020. The quarterly seasonality pattern in the number of daily announcements (top panel) is very clear. Weeks with a substantial number of dividend announcers are also associated with larger total dollar dividend payments (bottom panel).

Firms announce the suspension of dividend payments only once. This implies that a firm's dividend payments remain at zero in the following quarters (Q2 and Q3 2020) unless dividends are explicitly restarted. This information is missing from the CRSP data: when a firm does not announce a dividend, it is not reported as "zero" and will simply be missing. For the dividend suspenders, we therefore manually input in the remaining quarters of 2020 a dividend payment set equal to zero around the same date when these firms distributed a positive dividend in 2019, unless the firms restarted their dividend payments. This step is required to properly account for the continuation effect of dividend suspensions that last longer than a single quarter.

Our empirical analysis uses dividend growth from five industries, constructed using the methodology and industry definitions from Ken French's website: Industry 1 (Consumer goods): Consumer durables, nondurables, wholesale, retail, and some services (laundries, repair shops); Industry 2 (Manufacturing): Manufacturing, energy,

[4]Equation (1) uses the dollar amount of dividends paid by individual firms, implicitly applying value weights since large firms tend to have larger dividend payouts. As shown in Pettenuzzo et al. (2020), it makes little difference whether we use this measure or instead weight individual firms' dividend growth rates by their market capitalization.

[5]On two days in 2020 (March 30 and April 3 2020), the daily dividend announcements came exclusively from (three) dividend suspenders. For these cases we include the announcement on the previous day to avoid losing the information.

and utilities; Industry 3 (High Tech): Business equipment, telephone and television transmission; Industry 4 (Health): Healthcare, medical equipment, and drugs; and Industry 5 (Other): Mines, construction, building materials, transportation, hotels, business services, entertainment, and finance.

For each of these five industries, Figure 3 plots the growth rates $\Delta d_{t+1} = ln(G_{t+1})$ over the 2005-2020 sample (left column) and for the shorter 2020 sample (right column). The five series are dominated by large outliers, many of which can be attributed to shifts in the composition of firms announcing dividends on any given day, particularly on days with small numbers of announcing firms and a large proportion of dividend suspenders. During 2020, large, negative values of Δd_t occur more frequently after the pandemic lockdown in mid-March than prior to it and also tend to be more common across industries.

3 A Multivariate Dividend Growth Model

We next propose a multivariate econometric model that captures the salient features of the dynamics in the daily dividend growth data displayed in Figure 3 and the effect of dividend suspensions on the conditional (predictive) distribution of dividend growth. Our approach builds on the model developed in Pettenuzzo et al. (2020) but generalizes this model in three important ways. First, we develop a multivariate setting in which key components of the model (notably the persistent mean dynamics) can be correlated across variables. Second, we incorporate the effect of dividend suspensions on expected dividend growth, the conditional volatility of the dividend growth process, and the probability of observing jumps in dividends. Third, we introduce jumps in the dividend volatility process and allow these to be correlated with the jumps in the mean of the dividend growth process. These extensions, as we show, require material changes in the sampler used to estimate the model parameters and have an important impact on estimates of the dynamics in daily dividend growth.

3.1 Dividend Growth Dynamics

As shown in Figure 1 and Figure 2, daily values of announced dividend payments and dividend suspensions display substantial heterogeneity, reflecting variation in the number, size, and types of firms announcing dividend news on a given day. This makes it difficult to draw reliable conclusions from raw dividend data and requires us to adopt a sophisticated econometric modeling approach that is capable of extracting components from the dividend growth process that display very different dynamics and distributional features.

The econometric approach in Pettenuzzo et al. (2020) decomposes the aggregate daily dividend growth process, $\Delta d_{t+1} = \ln(G_{t+1})$, into three parts, namely (i) a persistent component, μ_{dt+1}, used to capture a smoothly evolving mean component; (ii) a jump component, $\xi_{dt+1}J_{dt+1}$, for which $J_{dt+1} \in \{0,1\}$ is a jump indicator that equals one when dividend growth experiences a jump on day $t+1$ and otherwise equals zero, and $\xi_{dt+1} \sim \mathcal{N}\left(0, \sigma_{\xi}^2\right)$ measures the magnitude of the jump; and (iii) a transitory shock, ε_{dt+1}, whose volatility can vary over time.

Here we are interested in extending the method to a multivariate setting which allows us to model jointly the dividend growth process across multiple industries and study possible cross-dependencies. With this in mind, let Δd_{t+1}^i denote the year-on-year dividend growth in industry i, with $i = 1, ..., K$, and stack the industry growth rates in the vector $\Delta \boldsymbol{d}_{t+1} = \left(\Delta d_{t+1}^1, ..., \Delta d_{t+1}^K\right)'$. Moreover, consistent with the previous discussion, specify the following model for this process:[6]

$$\Delta \boldsymbol{d}_{t+1} = \boldsymbol{\mu}_{dt+1} + \boldsymbol{\xi}_{dt+1} \odot \boldsymbol{J}_{dt+1} + \boldsymbol{\Sigma}_{dt+1}^{1/2} \boldsymbol{\varepsilon}_{dt+1}, \tag{2}$$

where $\boldsymbol{\mu}_{dt+1} = \left(\mu_{dt+1}^1, ..., \mu_{dt+1}^K\right)'$, $\boldsymbol{\xi}_{dt+1} = \left(\xi_{dt+1}^1, ..., \xi_{dt+1}^K\right)'$, $\boldsymbol{J}_{dt+1} = \left(J_{dt+1}^1, ..., J_{dt+1}^K\right)'$, $\boldsymbol{\varepsilon}_{dt+1} = \left(\varepsilon_{dt+1}^1, ..., \varepsilon_{dt+1}^K\right)' \sim \mathcal{N}\left(\boldsymbol{0}, \boldsymbol{I}_K\right)$ and $\boldsymbol{\Sigma}_{dt+1}$ is a $K \times K$ diagonal matrix.

We next discuss the motivation for these three components along with our assumptions about their behavior.

Starting with the vector of persistent mean components $\boldsymbol{\mu}_{dt+1}$, we allow for dynamics

[6] Here $\odot$ denotes the Hadamard product.

across variables by adopting a vector autoregressive setting that can capture lead-lag effects among the various industries. In addition, we include exogenous covariates that contain forward-looking information such as dividend suspensions.

Suspending dividends is not a decision that firms take lightly and we would not expect firms to stop making dividend payments if their cash flows are affected by a negative shock perceived to be short-lived. Hence, we would expect that there is additional signal value about the severity and longevity of a negative cash flow shock from firms' decision to suspend dividends. To account for these effects, we introduce the following VAR-X(1) process for the dynamics of $\boldsymbol{\mu}_{dt+1}$

$$\boldsymbol{\mu}_{dt+1} = \boldsymbol{\mu}_{\mu} + \boldsymbol{\Phi}_{\mu}\left(\boldsymbol{\mu}_{dt} - \boldsymbol{\mu}_{\mu}\right) + \boldsymbol{X}^{\mu}_{t+1}\boldsymbol{B}_{\mu} + \boldsymbol{\Sigma}^{1/2}_{\mu}\boldsymbol{\varepsilon}_{\mu t+1}, \quad \boldsymbol{\varepsilon}_{\mu t+1} \sim \mathcal{N}\left(\mathbf{0}, \boldsymbol{I}_K\right) \tag{3}$$

where

$$\boldsymbol{X}^{\mu}_{t+1} = \begin{bmatrix} \left(\boldsymbol{x}^{\mu}_{1,t+1}\right)' & \mathbf{0}' & \mathbf{0}' & \dots & \mathbf{0}' \\ \mathbf{0}' & \left(\boldsymbol{x}^{\mu}_{2,t+1}\right)' & \mathbf{0}' & \dots & \mathbf{0}' \\ \vdots & \vdots & \vdots & \ddots & \vdots \\ \mathbf{0}' & \mathbf{0}' & \mathbf{0}' & \dots & \left(\boldsymbol{x}^{\mu}_{K,t+1}\right)' \end{bmatrix} \tag{4}$$

can accommodate industry-specific as well as common exogenous regressors and $\boldsymbol{B}_{\mu} = \left(\boldsymbol{\beta}'_{1\mu}, ..., \boldsymbol{\beta}'_{K\mu}\right)'$ collects the associated coefficients. In our empirical application, we include as an extra covariate the market-wide proportion of firms suspending dividends, defined as $R_{st+1} = N_{st+1}/\left(N_{st+1} + N_{dt+1}\right)$, i.e. the ratio of the number of dividend suspenders, N_{st+1}, to the total number of dividend announcers (including suspenders), $(N_{st+1} + N_{dt+1})$. Hence, $\boldsymbol{X}^{\mu}_{t+1} = I_K \otimes R_{st+1}$ and $\boldsymbol{B}_{\mu} = \left(\beta_{1\mu}, ..., \beta_{K\mu}\right)'$. Negative values for $\beta_{i\mu}$ would indicate that a greater fraction of dividend suspenders is associated with a reduction in future dividend growth in industry i.[7]

Next, we focus on the processes controlling the jump intensities and timing. Because of large differences in both the dollar value of dividends paid by individual firms as well

[7]We elect to use the economy-wide suspension rate because this series is less noisy than the industry-level suspension rates which helps us obtain more accurate estimates. Moreover, cross-industry spillovers in $\boldsymbol{\mu}_{dt+1}$ are captured through the off-diagonal coefficients of $\boldsymbol{\Phi}_{\mu}$ (lagged effects) and $\boldsymbol{\Sigma}_{\mu}$ (contemporaneous effects). Finally, we would expect aggregate suspensions to identify an economy-wide effect better than industry-level suspension rates.

as in the number of firms announcing dividends on a given day, there is a higher probability of observing large outliers in the daily dividend growth rate on days with few announcers. Building on Pettenuzzo et al. (2020), we allow each industry's jump probability in (2) to depend on the number of total dividend announcers, N_{dt+1}. Moreover, we allow the proportion of total dividend suspenders, R_{st+1}, to affect each industry's jump intensity because days with a high proportion of dividend suspensions are more likely to be affected by firm-specific (idiosyncratic) dividend decisions. Finally, as in Johannes et al. (1999) we allow for state-dependency in the probability of jumps through lagged jumps, J^i_{dt}, and absolute values of total lagged dividend growth Δd_t.[8]

Combining these effects, we obtain the following jump probability specification:

$$\Pr\left(J^i_{dt+1}=1\middle|\,\boldsymbol{x}^J_{i,t+1}\right)=\Phi\left(\lambda_{i1}+\lambda_{i2}N_{dt+1}+\lambda_{i3}R_{st+1}+\lambda_{i4}J^i_{dt}+\lambda_{i5}\left|\Delta d_t\right|\right). \tag{5}$$

where $\boldsymbol{x}^J_{i,t+1}=\left(N_{dt+1},R_{st+1},J^i_{dt},|\Delta d_t|\right)$. We write the variance-covariance of the model $\boldsymbol{\Sigma}_{dt+1}=diag\left(e^{h^1_{dt+1}},...,e^{h^K_{dt+1}}\right)$, with

$$h^i_{dt+1}=\mu_{ih}+\phi_{ih}\left(h^i_{dt}-\mu_{ih}\right)+\xi^i_{ht+1}J^i_{dt+1}+\beta_{ih1}R_{st+1}+\beta_{ih2}\left|\Delta d_t\right|+\sigma_{ih}\varepsilon^i_{ht+1}, \tag{6}$$

where $\varepsilon^i_{ht+1}\sim\mathcal{N}\left(0,1\right)$.[9] As in (3), we include R_{st+1} as an extra covariate. In addition, we allow the magnitude of the previous day's dividend growth rate, $|\Delta d_t|$, to impact the log-volatility. Finally, as in Eraker et al. (2003), we allow the jumps in the mean and volatility of the dividend growth process to be correlated, with

$$\xi^i_{dt+1}\middle|\,\xi^i_{ht+1}\sim\mathcal{N}(\rho_{iJ}\xi^i_{ht+1},\sigma^2_{\xi^i_d}) \tag{7}$$

and

$$\xi^i_{ht+1}\sim\mathcal{N}(0,\sigma^2_{\xi^i_h}). \tag{8}$$

[8]While we assume that the observable covariates are common to all series, extending the model to allow for variable-specific covariates is trivial.

[9]We also require that $\varepsilon^i_{ht+1}\perp\varepsilon^j_{ht+1}$ for $i\neq j$, and that ε^i_{ht+1} is uncorrelated with both $\boldsymbol{\varepsilon}_{dt+1}$ and $\boldsymbol{\varepsilon}_{\mu t+1}$, for $i=1,...,K$, Finally, we assume that $|\phi_{ih}|<1$, $i=1,...,K$.

Consistent with our earlier stationarity assumptions, we specify the initial conditions for $\boldsymbol{\mu}_{dt}$ and $h^1_{dt}, ..., h^K_{dt}$ as[10]

$$\boldsymbol{\mu}_{d1} \sim \mathcal{N}\left(\boldsymbol{\mu}_{\mu} + \left(\boldsymbol{I}_K - \boldsymbol{\Phi}_{\mu}\right)^{-1} \boldsymbol{X}^{\mu}_1 \boldsymbol{B}_{\mu}, \boldsymbol{\Sigma}^{\dagger}_{\mu}\right), \tag{9}$$

with $\boldsymbol{\Sigma}^{\dagger}_{\mu}$ obtained by properly reshaping $\left(\boldsymbol{I}_{K^2} - \boldsymbol{\Phi}_{\mu} \otimes \boldsymbol{\Phi}_{\mu}\right)^{-1} \times vec\left(\boldsymbol{\Sigma}_{\mu}\right)$, and

$$h^i_{d1} \sim \mathcal{N}\left(\mu_{ih} + \frac{\beta'_{ih1}}{1-\phi_{ih}} R_{s1}, \frac{\sigma^2_{ih}}{1-\phi^2_{ih}}\right). \tag{10}$$

3.2 Priors

Starting with the parameters in (3), define $\boldsymbol{\phi}_{\mu} = vec\left(\boldsymbol{\Phi}'_{\mu}\right)$ and write[11]

$$\boldsymbol{\mu}_{\mu} \sim \mathcal{N}(\underline{\boldsymbol{\mu}}_{\mu 0}, \underline{\boldsymbol{V}}_{\mu_{\mu}}), \quad \boldsymbol{\phi}_{\mu} \sim \mathcal{N}(\underline{\boldsymbol{\phi}}_{\mu_0}, \underline{\boldsymbol{V}}_{\phi_{\mu}}) I(\boldsymbol{\phi}_{\mu} \in \mathcal{A}), \quad \boldsymbol{\Sigma}_{\mu} \sim \mathcal{IW}(\underline{\boldsymbol{S}}_{\mu}, \underline{V}_{\mu}). \tag{11}$$

Next, for $i = 1, ..., K$, we specify:

$$\mu_{ih} \sim \mathcal{N}(\underline{\mu}_{h0}, \underline{V}_{\mu_h}), \quad \phi_{ih} \sim \mathcal{N}(\underline{\phi}_{h_0}, \underline{V}_{\phi_h}) I(|\phi_{ih}| < 1), \quad \sigma^2_{ih} \sim \mathcal{IG}(\underline{V}_h, \underline{S}_h), \tag{12}$$

$$\sigma^2_{\xi^d_i} \sim \mathcal{IG}(\underline{V}_{\xi^d}, \underline{S}_{\xi^d}), \quad \sigma^2_{\xi^h_i} \sim \mathcal{IG}(\underline{V}_{\xi^h}, \underline{S}_{\xi^h}). \tag{13}$$

Finally, we define $\boldsymbol{\beta}_{ih} = (\beta_{ih1}, \beta_{ih2})'$ and $\boldsymbol{\lambda}_i = (\lambda_{i1}, ..., \lambda_{i5})'$ and write

$$\boldsymbol{\beta}_{i\mu} \sim \mathcal{N}(\underline{\boldsymbol{\beta}}_{\mu 0}, \underline{\boldsymbol{V}}_{\boldsymbol{\beta}_{\mu}}), \quad \boldsymbol{\beta}_{ih} \sim \mathcal{N}(\underline{\boldsymbol{\beta}}_{h0}, \underline{\boldsymbol{V}}_{\boldsymbol{\beta}_h}). \tag{14}$$

$$\boldsymbol{\lambda}_i \sim \mathcal{N}(\underline{\boldsymbol{\mu}}_{\boldsymbol{\lambda}}, \underline{\boldsymbol{V}}_{\boldsymbol{\lambda}}), \tag{15}$$

[10] We assume throughout that $J^i_{d0} = J^i_{d1} = 0$ and $\Delta d^i_0 = 0$, $i = 1, ..., K$.

[11] We use $\mathcal{A}$ to identify the set of restrictions on $\boldsymbol{\phi}_{\mu}$ that guarantees covariance stationarity of $\boldsymbol{\mu}_{dt+1}$, i.e. $\mathcal{A} \in R^{K \times K} : \max\left\{eig(\boldsymbol{\Phi}_{\mu})\right\} < 1$, where $\boldsymbol{\Phi}_{\mu}$ denotes the $K \times K$ matrix obtained by reshaping the $K^2 \times 1$ vector $\boldsymbol{\phi}_{\mu}$ appropriately.

and

$$\rho_{iJ} \sim \mathcal{N}\left(0, \underline{V}_{\rho}\right) \times I\left(\left|\rho_{iJ}\right| < 1\right). \tag{16}$$

In common with Pettenuzzo et al. (2020) our priors are loose and mildly uninformative with exception of ϕ_h^i $(i = 1, ..., K)$ and the diagonal elements of $\mathbf{\Phi}_\mu$, whose priors we center on 0.98, and the jump intensity variance $\sigma^2_{\xi_d^i}$, whose prior is centered on 3^2. We center the priors of ϕ_h^i $(i = 1, ..., K)$ and the diagonal elements of $\mathbf{\Phi}_\mu$ on a value just below unity in order to capture a small but highly persistent component in the mean of the dividend growth rate process.[12] Similarly, we choose a relatively high value for the prior of the jump intensity variance parameter $\sigma^2_{\xi_d^i}$ to better allow our model to distinguish between infrequent, large jumps and persistent stochastic volatility dynamics. For lower values of this prior, the component model tends to assign a large fraction of movements in dividend growth to small and medium-sized jumps and finds it difficult to separate between jumps and time-varying volatility. To capture the effect of dividend suspenders on estimates of aggregate dividend growth, we estimate the model both with and without dividend suspenders included.[13]

3.3 Estimation Methodology

We estimate our model using Bayesian Gibbs sampling and, to overcome the high computational costs introduced by both the daily data frequency and the multivariate nature of the model, we rely on a precision-based sampling approach.[14] We briefly describe how we obtain posterior estimates for the model parameters and latent state vectors. Throughout, we use compact notations $\boldsymbol{h}_d$, $\boldsymbol{\xi}_d$, $\boldsymbol{\xi}_h$, and $\boldsymbol{J}_d$ to denote the collection of $(T \times 1)$ vectors of log variances, jump intensities and locations across the K industries,

[12] This is consistent with a number of papers that estimate the parameters of stationary AR(1) processes such as those we employ to pin down time variation in our persistent mean component as well as in the stochastic volatility process, see, e.g., Clark and Ravazzolo (2015) and Chib et al. (2006).

[13] We exclude dividend suspenders by setting $I_t^i = 0$ for cases where firms announce that they have suspended dividends on day t.

[14] Precision-based sampling approaches for state-space models were first considered in Chan and Jeliazkov (2009) and McCausland et al. (2011). Their ease of implementation and computational efficiency makes these samplers very competitive. See Chan et al. (2021) for a recent summary of their applications in econometrics, ranging from dynamic factors models to macroeconomic forecasting.

i.e., $\boldsymbol{h}_d = \left\{\boldsymbol{h}_d^i\right\}_{i=1}^K$, $\boldsymbol{\xi}_d = \left\{\boldsymbol{\xi}_d^i\right\}_{i=1}^K$, $\boldsymbol{\xi}_h = \left\{\boldsymbol{\xi}_h^i\right\}_{i=1}^K$, and $\boldsymbol{J}_d = \left\{\boldsymbol{J}_d^i\right\}_{i=1}^K$. We also collect all the remaining parameters into the vector $\boldsymbol{\Theta}$,

$$\begin{aligned}\boldsymbol{\Theta} = \Big\{&\boldsymbol{\mu}_\mu, \boldsymbol{\Phi}_\mu, \boldsymbol{\Sigma}_\mu, \mu_{1h}, ..., \mu_{Kh}, \phi_{1h}, ..., \phi_{Kh}, \sigma_{1h}^2, ..., \sigma_{Kh}^2, \boldsymbol{\lambda}_1, ..., \boldsymbol{\lambda}_K, \sigma_{\xi_d^1}^2, ..., \sigma_{\xi_d^K}^2, \\ &\sigma_{\xi_h^1}^2, ..., \sigma_{\xi_h^K}^2, \boldsymbol{\beta}_{1\mu}, ..., \boldsymbol{\beta}_{K\mu}, \boldsymbol{\beta}_{1h}, ..., \boldsymbol{\beta}_{Kh}, \rho_{1J}, ..., \rho_{KJ}\Big\}.\end{aligned} \tag{17}$$

While the joint posterior distribution of all model parameters and latent state variables is highly non-linear, we can employ a Gibbs sampler algorithm augmented with a number of Metropolis-Hastings steps to draw recursively from the conditional posteriors of the model parameter and state variables. In particular, we break the evaluation of the joint posterior distribution into six blocks:

1. $\boldsymbol{\mu}_d \big| \, \boldsymbol{h}_d, \boldsymbol{\xi}_d, \boldsymbol{J}_d, \boldsymbol{\Theta}, \mathcal{D}^T$;
2. $\boldsymbol{h}_d^i \Big| \, \boldsymbol{\mu}_d^i, \boldsymbol{\xi}_d^i, \boldsymbol{\xi}_h^i, \boldsymbol{J}_d^i, \boldsymbol{\Theta}, \mathcal{D}^T \; (i = 1, ..., K)$;
3. $\boldsymbol{J}_d^i \Big| \, \boldsymbol{\mu}_d^i, \boldsymbol{\xi}_d^i, \boldsymbol{\xi}_h^i, \boldsymbol{h}_d^i, \boldsymbol{\Theta}, \mathcal{D}^T \; (i = 1, ..., K)$;
4. $\boldsymbol{\xi}_d^i \Big| \, \boldsymbol{\mu}_d^i, \boldsymbol{J}_d^i, \boldsymbol{\xi}_h^i, \boldsymbol{h}_d^i, \boldsymbol{\Theta}, \mathcal{D}^T \; (i = 1, ..., K)$;
5. $\boldsymbol{\xi}_h^i \Big| \, \boldsymbol{J}_d^i, \boldsymbol{h}_d^i, \boldsymbol{\Theta}, \mathcal{D}^T \; (i = 1, ..., K)$;
6. $\boldsymbol{\Theta} \big| \, \boldsymbol{\mu}_d, \boldsymbol{h}_d, \boldsymbol{\xi}_d, \boldsymbol{\xi}_h, \boldsymbol{J}_d, \mathcal{D}^T$.

Here $\mathcal{D}^T$ denotes the information set up to time T. The last block is further broken into twelve separate sub-blocks, one for each element of the parameter vector in (17).

The sampler presented above draws on the approach introduced in Pettenuzzo et al. (2020) but requires a number of important changes to allow for (i) joint modeling of the vector of industries' persistent mean components while allowing for contemporaneous correlation and lead-lag effects; (ii) state-dependency in the jump probability; (iii) exogenous regressors in the state equations of the persistent mean, log-variance, and jump probability components; (iv) jumps in the volatility process; (v) correlated jumps in

the mean and volatility processes; (vi) missing values in the industry dividend growth rates.[15] We refer the reader to Appendix A for further details.

At a high level, in addition to extending the original sampler to a multivariate setting, the posteriors of the jump probabilities of industry i, $\boldsymbol{J}_d^i$, which can simultaneously affect both the dividend growth and volatility, combine information from both processes. As a result, the posterior of J_{dt}^i now depends on both Δd_t and h_{dt}^i. In addition, the posteriors of the log-variances $\boldsymbol{h}_d^i$, which we compute using the data-augmentation approach of Kim et al. (1998), now depend on both the jump probabilities and intensities $\boldsymbol{J}_d^i$ and $\boldsymbol{\xi}_h^i$ as well as on the exogenous regressors in (6). This generalization requires a number of modifications to the mixture of normal approximation and data augmentation steps. Finally, the posterior of the correlation parameter ρ_{iJ}, which is restricted to lie between -1 and 1 through its prior, requires the introduction of an accept-reject step to avoid draws that violate this condition. These changes, in turn, trigger a large number of other modifications that affect the remaining blocks and steps in the sampler.

Here we focus on the first block, $\boldsymbol{\mu}_d | \, \boldsymbol{h}_d, \boldsymbol{\xi}_d, \boldsymbol{J}_d, \boldsymbol{\Theta}, \mathcal{D}^T$, which is novel, as well as the first three steps of the last block, $\boldsymbol{\Theta} | \, \boldsymbol{\mu}_d, \boldsymbol{h}_d, \boldsymbol{\xi}_d, \boldsymbol{\xi}_h, \boldsymbol{J}_d, \mathcal{D}^T$, which are related:

- $\boldsymbol{\mu}_\mu \Big| \, \boldsymbol{\mu}_d, \boldsymbol{\Theta}_{-\boldsymbol{\mu}_\mu}, \mathcal{D}^T$;
- $\boldsymbol{\Phi}_\mu \Big| \, \boldsymbol{\mu}_d, \boldsymbol{\Theta}_{-\boldsymbol{\Phi}_\mu}, \mathcal{D}^T$;
- $\boldsymbol{\Sigma}_\mu \Big| \, \boldsymbol{\mu}_d, \boldsymbol{\Theta}_{-\boldsymbol{\Sigma}_\mu}, \mathcal{D}^T$

Step 1: Start by rewriting the observation equation in (2) as follows:

$$\Delta \boldsymbol{d}^\star = \boldsymbol{Z}_\mu \boldsymbol{\mu}_d + \boldsymbol{\Sigma}_d^{1/2} \boldsymbol{\varepsilon}_d \quad \boldsymbol{\varepsilon}_d \sim \mathcal{N}(\boldsymbol{0}, \boldsymbol{I}_{TK}), \tag{18}$$

[15] To handle missing values, we follow a standard approach (see for example Durbin and Koopman (2012)) and work with a slightly modified state space representation which removes rows (and, when needed, columns too) that correspond to missing observations in our data.

where

$$\Delta \boldsymbol{d}^{\star} = vec\left(\begin{bmatrix} (\Delta \boldsymbol{d}_1 - \boldsymbol{\xi}_{d1} \odot \boldsymbol{J}_{d1})' \\ \vdots \\ (\Delta \boldsymbol{d}_T - \boldsymbol{\xi}_{dT} \odot \boldsymbol{J}_{dT})' \end{bmatrix}'\right), \tag{19}$$

$$\boldsymbol{Z}_{\mu} = \begin{bmatrix} 1 & & \\ & \ddots & \\ & & 1 \end{bmatrix} \quad \boldsymbol{\mu}_d = vec\left(\begin{bmatrix} \boldsymbol{\mu}'_{d1} \\ \vdots \\ \boldsymbol{\mu}'_{dT} \end{bmatrix}'\right) \quad \boldsymbol{\varepsilon}_d = vec\left(\begin{bmatrix} \boldsymbol{\varepsilon}'_{d1} \\ \vdots \\ \boldsymbol{\varepsilon}'_{dT} \end{bmatrix}'\right), \tag{20}$$

and

$$\boldsymbol{\Sigma}_d = \begin{bmatrix} \boldsymbol{\Sigma}_{d1} & & \\ & \ddots & \\ & & \boldsymbol{\Sigma}_{dT} \end{bmatrix}. \tag{21}$$

Next, combine the state equation for $\boldsymbol{\mu}_{dt+1}$ in (3) with the initial condition in (9) into:

$$\boldsymbol{H}_{\mu}\boldsymbol{\mu}_d = \widetilde{\delta}_{\mu} + \boldsymbol{\Omega}_{\mu}^{1/2}\boldsymbol{\varepsilon}_{\mu} \quad \boldsymbol{\varepsilon}_{\mu} \sim \mathcal{N}(\boldsymbol{0}, \boldsymbol{I}_{TK}), \tag{22}$$

where

$$\boldsymbol{H}_{\mu} = \begin{bmatrix} \boldsymbol{I}_k & \boldsymbol{0} & \dots & \dots & \boldsymbol{0} \\ -\boldsymbol{\Phi}_{\mu} & \boldsymbol{I}_k & \boldsymbol{0} & \cdots & \boldsymbol{0} \\ \vdots & \vdots & \vdots & \ddots & \vdots \\ \boldsymbol{0} & \dots & \boldsymbol{0} & -\boldsymbol{\Phi}_{\mu} & \boldsymbol{I}_k \end{bmatrix} \quad \widetilde{\delta}_{\mu} = \begin{bmatrix} \boldsymbol{\mu}_{\mu} + \left(\boldsymbol{I}_K - \boldsymbol{\Phi}_{\mu}\right)^{-1} \boldsymbol{X}_1^{\mu} \boldsymbol{B}_{\mu} \\ \left(\boldsymbol{I}_K - \boldsymbol{\Phi}_{\mu}\right) \boldsymbol{\mu}_{\mu} + \boldsymbol{X}_2^{\mu} \boldsymbol{B}_{\mu} \\ \vdots \\ \left(\boldsymbol{I}_K - \boldsymbol{\Phi}_{\mu}\right) \boldsymbol{\mu}_{\mu} + \boldsymbol{X}_T^{\mu} \boldsymbol{B}_{\mu} \end{bmatrix}, \tag{23}$$

and

$$\boldsymbol{\Omega}_{\mu} = \begin{bmatrix} \boldsymbol{\Sigma}_{\mu}^{\dagger} & & & \\ & \boldsymbol{\Sigma}_{\mu} & & \\ & & \ddots & \\ & & & \boldsymbol{\Sigma}_{\mu} \end{bmatrix} \tag{24}$$

Rearranging (22), we get

$$\boldsymbol{\mu}_d = \boldsymbol{\delta}_\mu + \boldsymbol{H}_\mu^{-1}\boldsymbol{\varepsilon}_\mu \tag{25}$$

where $\boldsymbol{\delta}_\mu = \boldsymbol{H}_\mu^{-1}\widetilde{\boldsymbol{\delta}}_\mu$. It follows that

$$\boldsymbol{\mu}_d \sim \mathcal{N}\left(\boldsymbol{\delta}_\mu, \left(\boldsymbol{H}_\mu'\boldsymbol{\Omega}_\mu^{-1}\boldsymbol{H}_\mu\right)^{-1}\right). \tag{26}$$

Finally, combining (18) and (26) leads to the following conditional posterior for $\boldsymbol{\mu}_d$:

$$\boldsymbol{\mu}_d \big| \boldsymbol{h}_d, \boldsymbol{\xi}_d, \boldsymbol{J}_d, \boldsymbol{\mu}_\mu, \boldsymbol{\Theta}, \mathcal{D}^T \sim \mathcal{N}(\overline{\boldsymbol{\mu}}_d, \overline{\boldsymbol{V}}_\mu) \tag{27}$$

where

$$\begin{aligned} \overline{\boldsymbol{V}}_\mu &= \left[\boldsymbol{H}_\mu'\boldsymbol{\Omega}_\mu^{-1}\boldsymbol{H}_\mu + \boldsymbol{Z}_\mu'\boldsymbol{\Sigma}_d^{-1}\boldsymbol{Z}_\mu\right]^{-1} \\ \overline{\boldsymbol{\mu}}_d &= \overline{\boldsymbol{V}}_\mu\left[(\boldsymbol{H}_\mu'\boldsymbol{\Omega}_\mu^{-1}\boldsymbol{H}_\mu)\boldsymbol{\delta}_\mu + \boldsymbol{Z}_\mu'\boldsymbol{\Sigma}_d^{-1}\Delta\boldsymbol{d}^\star\right]. \end{aligned} \tag{28}$$

Step 6, part 1: $\boldsymbol{\mu}_\mu \Big| \boldsymbol{\mu}_d, \boldsymbol{\Theta}_{-\boldsymbol{\mu}_\mu}, \mathcal{D}^T$

Start by combining (3) and (9) and rewriting them as

$$\boldsymbol{Z}_{\boldsymbol{\mu}_\mu} = \boldsymbol{W}_{\boldsymbol{\mu}_\mu}\boldsymbol{\mu}_d + \boldsymbol{\Omega}_\mu^{1/2}\boldsymbol{\varepsilon}_\mu \quad \boldsymbol{\varepsilon}_\mu \sim \mathcal{N}(\boldsymbol{0}, \boldsymbol{I}_{TK}), \tag{29}$$

where

$$\boldsymbol{Z}_{\boldsymbol{\mu}_\mu} = \begin{bmatrix} \boldsymbol{\mu}_{d1} - (\boldsymbol{I}_K - \boldsymbol{\Phi}_\mu)^{-1}\boldsymbol{X}_1^\mu\boldsymbol{B}_\mu \\ \boldsymbol{\mu}_{d2} - \boldsymbol{\Phi}_\mu\boldsymbol{\mu}_{d1} - \boldsymbol{X}_2^\mu\boldsymbol{B}_\mu \\ \vdots \\ \boldsymbol{\mu}_{dT} - \boldsymbol{\Phi}_\mu\boldsymbol{\mu}_{dT-1} - \boldsymbol{X}_T^\mu\boldsymbol{B}_\mu \end{bmatrix}, \quad \boldsymbol{W}_{\boldsymbol{\mu}_\mu} = \begin{bmatrix} \boldsymbol{I}_K \\ (\boldsymbol{I}_K - \boldsymbol{\Phi}_\mu) \\ \vdots \\ (\boldsymbol{I}_K - \boldsymbol{\Phi}_\mu) \end{bmatrix}. \tag{30}$$

Combining (29) with the prior for $\boldsymbol{\mu}_\mu$ in (11) leads to

$$\boldsymbol{\mu}_\mu \Big| \boldsymbol{\mu}_d, \boldsymbol{\Theta}_{-\boldsymbol{\mu}_\mu}, \mathcal{D}^T \sim \mathcal{N}(\overline{\boldsymbol{\mu}}_{\boldsymbol{\mu}_\mu}, \overline{\boldsymbol{V}}_{\boldsymbol{\mu}_\mu}), \tag{31}$$

where

$$\overline{\boldsymbol{V}}_{\mu_\mu} = \left[\underline{\boldsymbol{V}}_{\mu_\mu}^{-1} + \boldsymbol{W}_{\mu_\mu}'\boldsymbol{\Omega}_\mu^{-1}\boldsymbol{W}_{\mu_\mu}\right]^{-1}, \tag{32}$$

and

$$\overline{\boldsymbol{\mu}}_\mu = \overline{\boldsymbol{V}}_{\mu_\mu}\left[\underline{\boldsymbol{V}}_{\mu_\mu}\underline{\boldsymbol{\mu}}_{\mu 0} + \boldsymbol{W}_{\mu_\mu}'\boldsymbol{\Omega}_\mu^{-1}\boldsymbol{Z}_{\mu_\mu}\right]. \tag{33}$$

Step 6, part 2: $\boldsymbol{\Phi}_\mu \,|\, \boldsymbol{\mu}_d, \boldsymbol{\Theta}_{-\boldsymbol{\Phi}_\mu}, \mathcal{D}^T$

Start by rewriting (3) as

$$\boldsymbol{Z}_{t+1}^{\Phi_\mu} = \boldsymbol{W}_t^{\Phi_\mu}\boldsymbol{\phi}_\mu + \boldsymbol{\Sigma}_\mu^{1/2}\boldsymbol{\varepsilon}_{\mu t+1}, \tag{34}$$

where $\boldsymbol{\phi}_\mu = vec\left(\boldsymbol{\Phi}_\mu'\right)$,

$$\boldsymbol{Z}_{t+1}^{\Phi_\mu} = \boldsymbol{\mu}_{dt+1} - \boldsymbol{\mu}_\mu - \boldsymbol{X}_{t+1}^{\mu}\boldsymbol{B}_\mu, \tag{35}$$

and

$$\boldsymbol{W}_t^{\Phi_\mu} = \boldsymbol{I}_K \otimes \left(\boldsymbol{\mu}_{dt} - \boldsymbol{\mu}_\mu\right)'. \tag{36}$$

Following Kim et al. (1998), we start by obtaining a candidate draw for $\boldsymbol{\phi}_\mu$ from the following distribution:

$$\boldsymbol{\phi}_\mu^\star \sim \mathcal{N}\left(\overline{\boldsymbol{\phi}}_\mu, \overline{\boldsymbol{V}}_{\phi_\mu}\right), \tag{37}$$

where

$$\overline{\boldsymbol{V}}_{\phi_\mu} = \left[\underline{\boldsymbol{V}}_{\phi_\mu}^{-1} + \sum_{t=1}^{T-1}\left(\boldsymbol{W}_t^{\Phi_\mu}\right)'\boldsymbol{\Sigma}_\mu^{-1}\left(\boldsymbol{W}_t^{\Phi_\mu}\right)\right]^{-1}, \tag{38}$$

and

$$\overline{\boldsymbol{\phi}}_\mu = \overline{\boldsymbol{V}}_{\phi_\mu}\left[\underline{\boldsymbol{V}}_{\phi_\mu}^{-1}\underline{\boldsymbol{\phi}}_{\mu_0} + \sum_{t=1}^{T-1}\left(\boldsymbol{W}_t^{\Phi_\mu}\right)'\boldsymbol{\Sigma}_\mu^{-1}\boldsymbol{Z}_{t+1}^{\Phi_\mu}\right]. \tag{39}$$

Next, if the draw is retained, i.e. satisfies the stationarity restriction $I\left(\boldsymbol{\phi}_{\mu}^{*} \in \mathcal{A}\right)$, we accept $\boldsymbol{\phi}_{\mu}^{*}$ with probability $e^{\left(g\left(\boldsymbol{\phi}_{\mu}^{*}\right)-g\left(\boldsymbol{\phi}_{\mu}^{old}\right)\right)}$ where $\boldsymbol{\phi}_{\mu}^{old}$ is the retained draw from the previous iteration of the Gibbs sampler, and

$$g\left(\boldsymbol{\phi}_{\mu}\right) = \ln p\left(\boldsymbol{\phi}_{\mu}\right) + \frac{1}{2}\ln\left|\boldsymbol{\Sigma}_{\mu}^{\dagger}\right| - \frac{1}{2}\left\{\left(\boldsymbol{\mu}_{d1} - \boldsymbol{\mu}_{\mu} - \left(\boldsymbol{I}_{K} - \boldsymbol{\Phi}_{\mu}\right)^{-1}\boldsymbol{X}_{1}^{\mu}\boldsymbol{B}_{\mu}\right)'\left(\boldsymbol{\Sigma}_{\mu}^{\dagger}\right)^{-1}\right. \\ \left.\left(\boldsymbol{\mu}_{d1} - \boldsymbol{\mu}_{\mu} - \left(\boldsymbol{I}_{K} - \boldsymbol{\Phi}_{\mu}\right)^{-1}\boldsymbol{X}_{1}^{\mu}\boldsymbol{B}_{\mu}\right)\right\}, \tag{40}$$

with $p\left(\boldsymbol{\phi}_{\mu}\right)$ denoting the prior of $\boldsymbol{\phi}_{\mu}$ from (11) and as above $\boldsymbol{\Phi}_{\mu}$ denotes the $K \times K$ matrix obtained by reshaping $\boldsymbol{\phi}_{\mu}$ to conform with (3).

Step 6, part 3: $\boldsymbol{\Sigma}_{\mu}\left|\, \boldsymbol{\mu}_{d}, \boldsymbol{\Theta}_{-\boldsymbol{\Sigma}_{\mu}}, \mathcal{D}^{T}\right.$

Start by obtaining a candidate draw for $\boldsymbol{\Sigma}_{\mu}$ from the following distribution:

$$\boldsymbol{\Sigma}_{\mu}^{*} \sim \mathcal{IW}\left(\underline{V}_{\mu} + T - 1, \overline{\boldsymbol{S}}_{\mu}\right), \tag{41}$$

where

$$\overline{\boldsymbol{S}}_{\mu} = \underline{\boldsymbol{S}}_{\mu} + \sum_{t=1}^{T-1}\left(\boldsymbol{Z}_{t+1}^{\Phi_{\mu}} - \boldsymbol{W}_{t}^{\Phi_{\mu}}\boldsymbol{\phi}_{\mu}\right)\left(\boldsymbol{Z}_{t+1}^{\Phi_{\mu}} - \boldsymbol{W}_{t}^{\Phi_{\mu}}\boldsymbol{\phi}_{\mu}\right)'. \tag{42}$$

We accept $\boldsymbol{\Sigma}_{\mu}^{*}$ with probability $e^{\left(g\left(\boldsymbol{\Sigma}_{\mu}^{*}\right)-g\left(\boldsymbol{\Sigma}_{\mu}^{old}\right)\right)}$ where $\boldsymbol{\Sigma}_{\mu}^{old}$ is the retained draw from the previous iteration of the Gibbs sampler, and

$$g\left(\boldsymbol{\Sigma}_{\mu}\right) = \ln p\left(\boldsymbol{\Sigma}_{\mu}\right) + \frac{1}{2}\ln\left|\boldsymbol{\Sigma}_{\mu}^{\dagger}\right| - \frac{1}{2}\left\{\left(\boldsymbol{\mu}_{d1} - \boldsymbol{\mu}_{\mu} - \left(\boldsymbol{I}_{K} - \boldsymbol{\Phi}_{\mu}\right)^{-1}\boldsymbol{X}_{1}^{\mu}\boldsymbol{B}_{\mu}\right)'\left(\boldsymbol{\Sigma}_{\mu}^{\dagger}\right)^{-1}\right. \\ \left.\left(\boldsymbol{\mu}_{d1} - \boldsymbol{\mu}_{\mu} - \left(\boldsymbol{I}_{K} - \boldsymbol{\Phi}_{\mu}\right)^{-1}\boldsymbol{X}_{1}^{\mu}\boldsymbol{B}_{\mu}\right)\right\}, \tag{43}$$

with $p\left(\boldsymbol{\Sigma}_{\mu}\right)$ denoting the prior of $\boldsymbol{\Sigma}_{\mu}$ from (11).

4 Empirical Results

Having introduced our econometric approach, we next turn to our empirical results.

4.1 Parameter Estimates

Table 1 reports full-sample (January 2005–April 2020) estimates of the posterior mean, standard deviation and 90% credible sets for the parameters of the model (2)-(8). In line with historical data, our estimates of the implied unconditional mean ($\mu_{i\mu}$) suggest an annualized average dividend growth rate between 5.7% (Industry 3, high tech) and 8.7% (Industry 5, other). Estimates of the diagonal elements of Φ_μ are close to 0.98, implying that our approach extracts a highly persistent mean component from the daily dividend growth series. This component is very smooth at the daily frequency ($\Sigma_{\mu,ii}^{1/2}$ ranges from 0.005 to 0.007) compared to the far more volatile, temporary shocks to the dividend process (σ_{ih} ranges from 0.28 to 0.74).

Estimates of the off-diagonal terms of Φ_μ are small but quite precisely estimated. In particular, lagged values of μ_{dt} from Industry 5 (Others, including mines, finance and hotels) have a significantly positive effect on the μ_{dt} values of industries 1, 2, and 3. When added to the already highly persistent autoregressive (diagonal) terms, these spillover effects considerably increase the overall persistence of the μ_{dt} processes.

The stochastic volatility processes for daily dividend growth are far less persistent than the mean processes with ϕ_{ih} parameters ranging from 0.895 to 0.944. These values are also notably smaller than estimates commonly obtained for the volatility of daily stock returns. Dividend news can therefore not be the only source of volatility clustering in daily stock returns, suggesting either the presence of additional news sources or a complicated propagation mechanism related to the trading process itself.

Stochastic volatility in dividend growth is also strongly affected by jumps and the estimated variance parameters $\sigma_{\xi_h^i}$ are similar in magnitude to those of σ_{ih}. These jumps have an important effect on volatility dynamics during the pandemic.

Our estimates of the Probit specification for the jump process suggest that the jump component in the daily dividend growth series is highly volatile ($\sigma_{\xi_d^i} = 2.9$). For industries 1, 2, and 5, the negative and significant estimates of λ_{i2} show that jumps are significantly more likely to occur on days with a smaller number of dividend announcements. For industries 3 and 4 (high tech and health), these coefficient estimates

are not significant, however. The coefficients on the proportion of dividend suspenders, R_{st+1} are highly significant for four of five industries, the one exception being Industry 4 (health). Conversely, lagged jumps or lagged values of $|\Delta d_t|$ have no significant association with the subsequent jump probability for any of the industries. While jumps can simultaneously affect the mean and volatility of the daily dividend growth process, we find that the magnitudes of such movements are uncorrelated.

4.2 Suspensions and Dividend Growth Dynamics

Figure 4 plots the persistent dividend growth component μ_{dt+1} for the five industries computed with and without dividend suspensions in the model. We focus on 2020 because the two series are almost indistinguishable for the vast majority of the post-2005 sample, the only exception being a brief period during the GFC.

In the first two months of 2020, the two series are very similar as dividend suspensions are infrequent. However, from mid-March 2020 onward, we see a sharp divergence in the μ_{dt} estimates extracted from the two models: while the μ_{dt} estimates implied by the model that ignores dividend suspenders remain quite high or only decline very gradually during 2020, the μ_{dt} estimates from the generalized model that includes suspenders decline sharply for Industry 1 and 2 with the sharpest decline occurring from mid-March through April, 2020. By the end of April, μ_{dt} has fallen around 4% before it stabilizes or begins to slowly increase.

To further illustrate the impact of changes in the proportion of dividend suspenders on the dynamics of daily dividend growth, we proceed to compute long-run responses of dividend growth, volatilities, and jump probabilities with respect to changes in R_{st+1}. Estimating these long run effects in a highly non-linear model such as ours is far from simple. As discussed in Gallant et al. (1993) and Koop et al. (1996), these responses are both history- and shock-dependent and so their computation requires special care. To deal with this, we follow the approach in Gallant et al. (1993), and compute "representative", or average, response sequences using Monte Carlo integration. In particular, we begin by initializing all the conditioning variables at their sample means and proceed by permanently altering the fraction of dividend suspenders. Next, for each

component of the dividend process, we simulate S realizations of the persistent component, volatility, jump probability, and jump intensities, denoted by $\{\mu^s_{dT+H}\}^S_{s=1}$, $\{\exp\left(h^s_{dT+H}/2\right)\}^S_{s=1}$, $\{J^s_{dT+H}\}^S_{s=1}$, $\{\xi^s_{dT+H}\}^S_{s=1}$, $\{\xi^s_{hT+H}\}^S_{s=1}$, where $s = 1, ..., S$ indexes the simulation and H is the horizon.

Our approach accounts for parameter uncertainty since all parameters and latent states in the model (including the mean, volatility, and jump components) are treated as random variables. In particular, instead of iterating forward on the various processes by setting the parameter estimates of the dividend growth model at their respective posterior means, we follow Koop (1996) and draw from the entire (posterior) distribution of these parameters.

Results from this exercise are reported in the left column in Figure 5 which sets $H =$ 252 days and changes R_{st+1} from 0 to 50%. For stocks in Industry 1, μ_{dt} drops from around 0.08 to -0.05 as we increase R_{st+1} from zero to 50%. Conversely, in Industry 5 μ_{dt} only declines from 0.08 to 0.06 as R_{st+1} is reduced from zero to 50%.

The proportion of dividend suspensions also has a large effect on the jump probability. The right column in Figure 5 plots industry-level jump probabilities as a function of R_{st+1}, again fixing the other terms in (5) at their historical averages. Reflecting the heterogeneity in the estimates of λ_{i3}, results vary widely across industries. For example, as we vary the proportion of suspenders from zero to 50%, the jump probability increases from 5% to nearly 40% for consumer goods stocks (Industry 1), but only from 5% to less than 10% for industry 4 (health care).

The empirical analysis conducted here is made possible by our bottom-up approach which allows us to compute the direct effect of dividend suspenders on dividend growth expectations. Aggregate top-down approaches do not distinguish between smaller dividends arising from dividend reductions versus dividend suspensions. To see this, consider a case with two equally-sized companies (A and B), both paying \$10 million in dividends the previous year. In one scenario, company A doubles its dividends to \$20m, while company B suspends dividends. In another scenario, the two companies both maintain dividends at \$10m. From a top-down perspective, the two scenarios are identical because aggregate dividends are the same (\$20m). However, this clearly

ignores the signal value from company B suspending its dividends. Our empirical analysis demonstrates that this distinction can be very important for some industries such as consumer goods and manufacturing, though it matters less for industries such as high tech and health stocks.

4.3 Specification Analysis

To better understand the need for all three components in our dynamic econometric specification, we next examine the behavior of these components as we alter the model specification.

To understand the need for the jump and SV components, Figure 6 presents QQ plots for our model along with those generated using a model without these two components and, for reference, a 45 degree line representing a perfect fit. The figure clearly demonstrates how important the jump and SV components are: the model without these components completely misses the large outliers in the left and right tails across all industries.

Because all three latent components of our model are intricately linked, removing any one of them will affect the other components which will attempt to make up for the absence of a component. This will affect the extent to which the individual components can be interpreted economically and their ability to capture specific features of the dividend growth process. We next illustrate this point through a set of plots.

Figure 7 plots the extracted mean component μ_{dt} from our full model (benchmark) versus that from a model with (i) no jumps (top row); (ii) no SV (middle row); or (iii) no jumps and no SV (bottom row). The left column shows results for Industry 1 (consumer goods) while the right column shows results for Industry 5 (Other). Omitting jumps (top row) makes the μ_{dt} process much noisier, introducing many small, jittery movements that quickly reverse themselves and reduce the persistence in the process, particularly for consumer goods stocks. Still, the mean process extracted from the model without jumps clearly trails the baseline model. Keeping jumps, but removing the SV component (middle row) leads to similar differences relative to the benchmark model, although at times the two series differ by more than what we see in the top panels. Removing both

jumps and SV dynamics (bottom panel) generates a μ_{dt} process that is much more volatile and fluctuates over a wider range of values than the baseline model with notable swings in 2008/09, 2012, and 2013.

These plots show that removing any one of the jump or SV components (but not both) leads to noisier estimates of the persistent dividend growth component. Removing both components has a much greater impact, leading to notably bigger swings in the persistent dividend growth component extracted from the data.

Next, consider how removing the jump component affects the stochastic volatility component extracted from the data. The top row in Figure 8 plots the log volatility component for the baseline model and compares it to a model with no jumps. Leaving out jumps results in a volatility process that is dominated by multiple large spikes that immediately reverse themselves. This makes the extracted volatility process less smooth and more difficult to interpret and use for prediction purposes.

Removing the SV component in turn also affects the extracted jump component. To see this, the bottom row of Figure 8 shows the time series of the extracted jump components from the baseline model versus that of a model which excludes the SV component. While the processes are reasonably similar, we also notice the much higher incidence of jumps for Industry 5 (which includes financial firms) during the GFC and the Eurozone crisis (2011).

4.4 Dividend Growth Volatility and Uncertainty Measures

For each of the five industries, the left panels in Figure 9 plot the daily dividend growth volatility along with the aggregate stock market volatility (as measured by the VIX) and a proxy for economic policy uncertainty (Baker et al. (2016)). For industries 1, 2, and 5, dividend growth volatility spikes sharply in mid-March. Such spikes do not occur for industries 3 and 4 (high tech and health care) whose firms were less affected by the Covid pandemic. We also see local, industry-specific rises in volatility in May and August/September, though again this varies considerably across industries.

These patterns in dividend growth volatility can be compared to the evolution in the VIX. In normal markets, we would expect firms to deliberate on dividend suspension

decisions over an extended period of time, suggesting that stock market volatility should lead dividend volatility by a lengthy margin. In fact, the mid-March spikes in volatility of daily dividend growth for industries 1, 2 and 5 only trails the VIX by a few days, indicating the speed with which firms changed their dividend policies during the pandemic.

In the earliest phase of the pandemic that lasted up to late March, the Economic Policy Uncertainty index of Baker et al. (2016) closely follows our dividend volatility estimate that accounts for suspensions. However, while dividend volatility drops sharply in early April, economic policy uncertainty remains elevated until late May and stays well above its pre-pandemic level throughout the summer and early fall of 2020.

We conclude that the VIX, Economic Policy Uncertainty index, and dividend growth volatility measures for 3 of the 5 industries all reached highly abnormal levels in the days after the pandemic lockdown. While the spike in the VIX preceded that of the dividend growth volatility measure, it only did so by a few days, indicating the speed with which companies adjusted their dividend policies. Our results also demonstrate considerable heterogeneity in dividend growth volatility across the five industries, reflecting the very different impact the pandemic lockdown had on cash flows in different industries.

4.5 Dividend Growth Estimates and Market Volatility

To formally analyze the lead-lag relation between the VIX and the stochastic volatility component extracted from our daily dividend growth measure with (SV_t^{sus}) and without (SV_t^{no-sus}) suspenders, we next estimate a set of simple linear models that include a few lags of these variables:

$$VIX_t = \alpha^{VIX} + \sum_{j=1}^{3} \beta_j^{VIX} VIX_{t-j} + \sum_{j=1}^{3} \gamma_j^{VIX} SV_{t-j} + \varepsilon_t^{VIX}, \tag{44}$$

$$SV_t = \alpha^{SV} + \sum_{j=1}^{3} \beta_j^{SV} VIX_{t-j} + \sum_{j=1}^{3} \gamma_j^{SV} SV_{t-j} + \varepsilon_t^{SV}, \tag{45}$$

where SV_t refers to either SV_t^{sus} or SV_t^{no-sus}. Our regressions include three daily lags but our empirical results are not sensitive to this choice. Because the VIX measures the

volatility for the overall stock market, these predictive regressions use real-time volatility estimates from a univariate model estimated on aggregate dividends.[16]

Table 2 reports results from various versions of these regressions. First consider the regression in (44) that uses the VIX as the dependent variable and only includes its own lags. As shown in column (1), the first three lags of the VIX account for 92.5% of the variation in next day's VIX. Omitting lags of the VIX, lagged daily values of the dividend volatility estimates that account for suspensions are highly statistically significant, although they only explain a little under 17% of the variation in the VIX. Interestingly, the three lags of SV^{sus} maintain their joint statistical significance even after including the lagged values of the VIX (column 4). This is a strong result given the finding in Paye (2012) that few variables are capable of predicting movements in the VIX after accounting for lagged values of the VIX. The marginal increase in the adjusted R^2 of the VIX regression due to the inclusion of lags of SV^{sus} is quite small, however, provided that lags of the VIX are also conditioned on.

In sharp contrast, the dividend volatility estimate that ignores suspenders (SV_t^{no-sus}) has no predictive power over the VIX neither when appearing on its own (column 3) or in combination with lags of the VIX (column 5). In fact, SV^{no-sus} generates a negative value of the adjusted R^2 value (-1.52%) in the first of these regressions.

Turning to the reverse regressions that use dividend volatility as the dependent variable (45), lagged values of the VIX explain around 30% of the daily variation in SV^{sus} during our sample (column 6), which is substantially lower than the 49% explained by lagged values of SV^{sus} (column 7). Adding lags of the VIX to lags of SV^{sus} marginally increases the adjusted R^2 from 49% to 52% (column 8).

Real-time estimates of dividend growth volatility based on the model that ignores dividend suspensions are far less persistent and bear little relation to the VIX. In fact, lagged values of the VIX fail to be (jointly) significant in regressions that use SV^{no-sus} as the dependent variable. Even lagged values of SV^{no-sus} have no predictive power over future values, suggesting that estimation error in the real-time estimates of this variable

[16]Parameter estimates for this aggregate model with and without dividend suspenders are reported in Table B.1, while real-time estimates of μ_{dt} and $\exp(h_{dt}/2)$ are displayed in Figure B.1. Conversely, the industry-level volatility values are based on full-sample estimates.

dampens any underlying persistence.

4.6 Variation in Dividend Futures Prices

Stock prices reflect investors' views on the discounted present value of all future dividend payments, including payments that occur in the distant future. However, there is also a market for dividend futures whose prices incorporate investor expectations about dividend payments in the near-future, e.g., the calendar year 2020 or 2021. Examining this market during the early stage of the Covid-19 pandemic, Gormsen and Koijen (2020) find that investors sharply reduced their expectations of near-term dividend payments.

To explore the link between our dividend growth estimates and prices in this market, we obtain daily data on dividend futures from the Chicago Mercantile Exchange (CME) which tracks the annual dividends paid by companies in the S&P 500 at different maturities. We focus on the two most liquid and directly impacted dividend futures with maturity dates of December 2020 and December 2021.

The right column in Figure 9 plots volatility estimates from GARCH(1,1) models fitted to the daily returns of these dividend futures contracts along with our five industry-level dividend growth volatility estimates. We see clear similarities between the sharp mid-March peak in our dividend volatility estimates for Industries 1, 2 and 5 particularly versus the December 2021 contract. In contrast with our SV estimates, however, dividend futures volatility declines largely monotonically for the remainder of our sample.

To further examine links between news in the dividend futures market and estimates of the dividend growth components from our econometric model, Table 3 presents regressions of daily returns on the two dividend futures contracts on concurrent (same-day) estimates of the mean, variance and jump components extracted from our model. The first row presents results from a model that uses real-time estimates obtained from the earlier univariate model fitted to the aggregate dividend data while rows 2-6 report results for the five individual industries. In each case, we report slope coefficients, t-statistics, and R^2 values from univariate regressions that use daily returns on the futures contracts as the dependent variable and an intercept and one of the components

from our dividend growth model as regressor.

Upward revisions in the persistent dividend growth component $\Delta\mu_{dt}$ for industries 1 and 2 are significantly positively correlated with returns on both dividend futures contracts. This is consistent with dividend futures reacting positively to the same growth news that our μ_{dt} component tracks. Conversely, the aggregate volatility component extracted from our model, $\exp(h_{dt})$, is significantly *negatively* correlated with returns on both dividend futures contracts. This is consistent with the common finding that returns and volatility move in opposite directions since higher uncertainty raises risk premia. Finally, the jump component for Industry 5 (Other, including financial firms) is significantly positively correlated with dividend futures contracts, with very high R^2 values. This reflects the large negative jumps to dividend growth during the early stage of the pandemic (Figure 3) which occurred on the same days that returns on dividend futures were sharply negative.[17]

5 Conclusion

We develop a multivariate dynamic econometric model and an associated MCMC sampling approach that helps us extract estimates of persistent mean, stochastic volatility and jump components which are salient features of the daily dividend growth process and played an important role during the Covid-19 pandemic. Our empirical estimates suggest that dividend suspensions had a sizeable impact on the distribution of dividend growth in industries such as consumer goods and manufacturing while they had less of an impact on the high tech and healthcare industries during the pandemic.

Our econometric approach is likely to prove valuable for handling other data sets with features similar to those observed for daily dividend growth. In particular, outliers (jumps), correlated dynamics, and time-varying volatility are features of time series with considerable cross-sectional heterogeneity such as house prices or inflation rates for different categories of goods and services. For such variables, the underlying persistent

[17] Figure B.2 shows daily returns on the dividend futures contracts expiring on December 2020 and December 2021. Returns were sharply negative on most days in the second half of March.

(predictive) component is often quite small and extracting an accurate estimate of it requires handling outliers and time-varying volatility.

References

ALBERT, J. H. AND S. CHIB (1993): "Bayesian Analysis of Binary and Polychotomous Response Data," *Journal of the American Statistical Association*, 88, 669–679.

ATKESON, A. (2020): "What will be the economic impact of covid-19 in the US? Rough estimates of disease scenarios," *Working Paper*.

BAKER, S. R., N. BLOOM, AND S. J. DAVIS (2016): "Measuring Economic Policy Uncertainty," *The Quarterly Journal of Economics*, 131(4), 1593–1636.

CHAN, J. C., A. POON, AND D. ZHU (2021): "Efficient Estimation of State-Space Mixed-Frequency VARs: A Precision-Based Approach," *arXiv preprint arXiv:2112.11315*.

CHAN, J. C. C. AND I. JELIAZKOV (2009): "Efficient simulation and integrated likelihood estimation in state space models," *International Journal of Mathematical Modelling and Numerical Optimisation*, 1, 101–120.

CHIB, S., F. NARDARI, AND N. SHEPHARD (2006): "Analysis of high dimensional multivariate stochastic volatility models," *Journal of Econometrics*, 134(2), 341–371.

CLARK, P. (1973): "A Subordinated Stochastic Process Model with Finite Variance for Speculative Prices," *Econometrica*, 41, 135–55.

CLARK, T. E. AND F. RAVAZZOLO (2015): "Macroeconomic forecasting performance under alternative specifications of time-varying volatility," *Journal of Applied Econometrics*, 30, 551–575.

DURBIN, J. AND S. J. KOOPMAN (2012): *Time Series Analysis by State Space Methods (Second Edition)*, Oxford University Press, Oxford.

EICHENBAUM, M. S., S. REBELO, AND M. TRABANDT (2020): "The Macroeconomics of Epidemics," *Working Paper*.

ERAKER, B., M. JOHANNES, AND N. POLSON (2003): "The Impact of Jumps in Volatility and Returns," *The Journal of Finance*, 58, 1269–1300.

GALLANT, A. R., P. E. ROSSI, AND G. TAUCHEN (1993): "Nonlinear Dynamic Structures," *Econometrica*, 61(4), 871–907.

GORMSEN, N. J. AND R. S. KOIJEN (2020): "Coronavirus: Impact on Stock Prices and Growth Expectations," *The Review of Asset Pricing Studies*, 10(4), 574–597.

GOURINCHAS, P.-O. (2020): "Flattening the Pandemic and Recession Curves," *Working Paper*.

JOHANNES, M., R. KUMAR, AND N. G. POLSON (1999): "State Dependent Jump Models: How do US Equity Indices Jump?" *Working Paper*.

KIM, S., N. SHEPHARD, AND S. CHIB (1998): "Stochastic Volatility: Likelihood Inference and Comparison with ARCH Models," *The Review of Economic Studies*, 65(3), 361–393.

KOOP, G. (1996): "Parameter uncertainty and impulse response analysis," *Journal of Econometrics*, 72(1), 135–149.

KOOP, G., M. PESARAN, AND S. M. POTTER (1996): "Impulse response analysis in nonlinear multivariate models," *Journal of Econometrics*, 74(1), 119–147.

LUDVIGSON, S. C., S. MA, AND S. NG (2020): "COVID19 and The Macroeconomic Effects of Costly Disasters," *Working Paper*.

MCCAUSLAND, W. J., S. MILLER, AND D. PELLETIER (2011): "Simulation smoothing for state-space models: A computational efficiency analysis," *Computational Statistics and Data Analysis*, 55, 199–212.

PAYE, B. S. (2012): "'Déjà vol': Predictive regressions for aggregate stock market volatility using macroeconomic variables," *Journal of Financial Economics*, 106, 527 – 546.

PETTENUZZO, D., R. SABBATUCCI, AND A. TIMMERMANN (2020): "Cash Flow News and Stock Price Dynamics," *The Journal of Finance*, 75, 2221–2270.

Parameter estimates

	Ind 1				Ind 2				Ind 3				Ind 4				Ind 5			
	Mean	*Std*	*90% C.S.*		*Mean*	*Std*	*90% C.S.*		*Mean*	*Std*	*90% C.S.*		*Mean*	*Std*	*90% C.S.*		*Mean*	*Std*	*90% C.S.*	
$\mu_{i\mu}$	0.074	0.008	0.061	0.086	0.068	0.006	0.058	0.078	0.057	0.006	0.047	0.067	0.061	0.005	0.053	0.069	0.087	0.012	0.067	0.106
$\Sigma^{1/2}_{\mu,ii}$	0.005	0.000	0.004	0.006	0.005	0.000	0.004	0.005	0.005	0.001	0.004	0.006	0.005	0.001	0.004	0.006	0.007	0.001	0.006	0.008
μ_{ih}	-4.946	0.133	-5.165	-4.732	-5.193	0.137	-5.431	-4.966	-4.790	0.145	-5.027	-4.555	-5.237	0.140	-5.457	-5.014	-4.356	0.170	-4.635	-4.072
ϕ_{ih}	0.922	0.009	0.907	0.937	0.895	0.008	0.881	0.909	0.911	0.009	0.897	0.925	0.944	0.008	0.930	0.957	0.903	0.009	0.888	0.918
σ_{ih}	0.457	0.054	0.368	0.547	0.682	0.053	0.595	0.774	0.564	0.062	0.456	0.670	0.281	0.046	0.210	0.357	0.738	0.065	0.633	0.839
$\sigma^i_{\xi_d}$	2.853	0.044	2.782	2.927	2.892	0.045	2.818	2.968	2.897	0.044	2.827	2.970	2.945	0.045	2.873	3.023	2.869	0.043	2.799	2.942
$\sigma^i_{\xi_h}$	0.634	0.068	0.525	0.751	0.670	0.085	0.541	0.814	0.669	0.088	0.539	0.822	0.899	0.142	0.677	1.155	0.635	0.079	0.519	0.770
λ_{i1}	-1.275	0.063	-1.377	-1.170	-1.542	0.068	-1.659	-1.431	-1.463	0.075	-1.589	-1.342	-1.709	0.108	-1.892	-1.536	-1.268	0.062	-1.372	-1.168
λ_{i2}	-0.048	0.014	-0.072	-0.026	-0.025	0.011	-0.043	-0.007	-0.010	0.020	-0.044	0.024	0.092	0.054	0.005	0.179	-0.017	0.005	-0.026	-0.009
λ_{i3}	2.974	0.634	2.006	4.055	1.834	0.721	0.625	3.061	1.843	0.720	0.667	3.043	0.814	1.224	-1.322	2.679	1.995	0.554	1.103	2.921
λ_{i4}	0.087	0.126	-0.124	0.287	-0.106	0.172	-0.398	0.165	-0.303	0.186	-0.622	-0.001	-0.131	0.343	-0.743	0.390	-0.109	0.130	-0.323	0.097
λ_{i5}	-0.056	0.084	-0.203	0.064	0.074	0.059	-0.027	0.168	0.014	0.097	-0.152	0.159	-0.335	0.269	-0.819	0.031	-0.030	0.101	-0.220	0.113
$\beta_{i\mu}$	-0.005	0.002	-0.009	-0.002	-0.001	0.002	-0.004	0.002	-0.001	0.002	-0.005	0.003	-0.002	0.002	-0.006	0.002	-0.001	0.003	-0.006	0.004
β_{ih1}	0.054	0.218	-0.308	0.402	0.357	0.309	-0.199	0.823	-0.443	0.297	-1.002	-0.016	-0.084	0.145	-0.327	0.147	0.205	0.243	-0.193	0.611
β_{ih2}	0.042	0.035	-0.016	0.100	-0.043	0.047	-0.123	0.035	0.043	0.047	-0.032	0.119	0.008	0.031	-0.042	0.058	0.012	0.058	-0.085	0.105
ρ_{iJ}	-0.003	0.097	-0.164	0.152	-0.001	0.095	-0.159	0.158	-0.001	0.096	-0.163	0.159	0.001	0.075	-0.126	0.120	-0.016	0.100	-0.180	0.154

	Mean					5pct					95pct				
	$\Phi_\mu(.,1)$	$\Phi_\mu(.,2)$	$\Phi_\mu(.,3)$	$\Phi_\mu(.,4)$	$\Phi_\mu(.,5)$	$\Phi_\mu(.,1)$	$\Phi_\mu(.,2)$	$\Phi_\mu(.,3)$	$\Phi_\mu(.,4)$	$\Phi_\mu(.,5)$	$\Phi_\mu(.,1)$	$\Phi_\mu(.,2)$	$\Phi_\mu(.,3)$	$\Phi_\mu(.,4)$	$\Phi_\mu(.,5)$
$\Phi_\mu(.,1)$	0.980	0.004	0.001	0.000	0.010	0.979	0.001	-0.003	-0.004	0.005	0.980	0.008	0.005	0.004	0.016
$\Phi_\mu(.,2)$	0.007	0.979	0.002	0.001	0.009	0.002	0.979	-0.004	-0.005	0.002	0.013	0.980	0.008	0.007	0.016
$\Phi_\mu(.,3)$	0.002	0.002	0.979	0.002	0.009	-0.004	-0.003	0.979	-0.004	0.002	0.008	0.006	0.979	0.008	0.016
$\Phi_\mu(.,4)$	0.000	0.002	0.000	0.979	0.003	-0.006	-0.003	-0.005	0.979	-0.004	0.005	0.006	0.006	0.980	0.011
$\Phi_\mu(.,5)$	0.003	0.004	0.003	0.002	0.980	0.000	0.001	0.000	-0.002	0.979	0.006	0.006	0.006	0.005	0.980

Table 1: Parameter estimates for the dividend growth rate model. This table shows parameter estimates for the model that accounts for dividend suspenders fitted to the daily dividend growth as described in Section 3.

Volatility Predictive Regressions

	VIX_{t+1}					$SVOL_{sus,t+1}$			$SVOL_{no-sus,t+1}$		
	(1)	(2)	(3)	(4)	(5)	(6)	(7)	(8)	(9)	(10)	(11)
VIX_t	.654***			.621***	.652***	-.009		.004	-.001		-.000
	[6.30]			[4.76]	[6.36]	[-0.98]		[0.41]	[-0.53]		[-0.20]
VIX_{t-1}	.408***			.433***	.411***	.002		-.002	-.001		-.001
	[3.00]			[3.24]	[2.98]	[0.39]		[-0.25]	[-0.91]		[-0.96]
VIX_{t-2}	-.097			-.059	-.096	.022***		.005	.003		.002
	[1.43]			[-0.65]	[-1.38]	[3.49]		[1.22]	[1.38]		[0.99]
$SVOL_{sus,t}$		8.200**		-2.162**			.417***	.351***			
		[2.23]		[-2.31]			[4.48]	[4.30]			
$SVOL_{sus,t-1}$		5.960***		1.310***			.209***	.164**			
		[3.59]		[2.74]			[3.09]	[3.22]			
$SVOL_{sus,t-2}$		2.505		-1.436***			.175*	.148**			
		[1.15]		[-2.82]			[1.81]	[1.81]			
$SVOL_{no-sus,t}$			2.131		-1.946					.152	.148
			[0.26]		[-1.33]					[1.61]	[1.63]
$SVOL_{no-sus,t-1}$			2.918		1.584					.058	.053
			[0.35]		[0.60]					[1.58]	[1.48]
$SVOL_{no-sus,t-2}$			.438		-1.293					-.025	-.024
			[0.06]		[-0.82]					[-0.76]	[-0.74]
adj. R^2	92.55%	16.93%	-1.52%	92.83%	92.38%	30.55%	49.01%	52.09%	-0.40%	1.27%	0.12%
F − test VIX block (p-value)	0.00	-	-	0.00	0.00	0.00	-	0.01	0.53	-	0.69
F − test SVOL block (p-value)	-	0.00	0.06	0.00	0.55	-	0.00	0.00	-	0.05	0.05
Observations	186	186	183	186	183	186	186	186	185	182	182

Table 2: Volatility predictive regressions. This table shows estimates of daily predictive regressions for the VIX (columns 1-5), a stochastic volatility measure taking into account dividend suspenders (columns 6-8), and a stochastic volatility measure that does not take into accounts the dividend suspenders (columns 9-11) using three lags of the variables. The *F*-test reports the *p*-value of the joint null hypothesis that the "block" (e.g., three) coefficients on lagged VIX or stochastic volatility are zero. Newey-West s.e. (5 lags). The sample period is from January 2020 to September 2020.

	ret_t^{2020}			ret_t^{2021}		
	(1)	(2)	(3)	(4)	(5)	(6)
	$\Delta\mu_{dt}$	$\exp(h_{dt})$	J_{dt}	$\Delta\mu_{dt}$	$\exp(h_{dt})$	J_{dt}
Aggregate	.303	-.004***	.001	.443	-.001**	.001
	[1.09]	[-6.47]	[0.35]	[1.52]	[-2.32]	[0.15]
	2.86%	15.26%	0.13%	2.92%	0.59%	0.04%
Industry 1	2.961*	-0.048	-.001**	4.443**	-.029	.000
	[1.74]	[-0.84]	[-2.21]	[2.11]	[-0.36]	[0.15]
	4.43%	0.70%	0.35%	4.75%	0.12%	0.01%
Industry 2	4.144**	.111	.001	9.122***	.190	.000
	[2.56]	[0.84]	[1.27]	[2.72]	[1.26]	[0.57]
	3.04%	2.44%	0.29%	7.01%	3.44%	0.02%
Industry 3	2.468*	0.084	.000	3.627	.072	.001*
	[1.96]	[0.83]	[0.07]	[1.63]	[0.52]	[1.92]
	1.58%	0.21%	0.00%	1.62%	0.07%	0.05%
Industry 4	2.101	.213	.000	2.911	.421	-.002
	[0.99]	[1.07]	[0.50]	[1.18]	[1.18]	[-0.82]
	1.11%	0.31%	0.01%	1.02%	0.58%	0.02%
Industry 5	.369	-.115*	.011**	-1.300	-.026	.022**
	[0.69]	[-1.90]	[2.34]	[-1.54]	[-0.55]	[2.03]
	0.06%	6.88%	8.70%	0.33%	0.17%	18.73%

Table 3: Regressions of dividend futures returns on the estimated dividend growth components $\Delta\mu_{dt}$, $\exp(h_{dt})$ and J_{dt}. This table presents estimates of the regression of dividend futures returns on $\Delta\mu_{dt}$, $\exp(h_{dt})$ and J_{dt} at the aggregate and industry levels. Columns (1)-(3) report results for the dividend futures expiring on December 2020, while columns (4)-(6) for the one expiring on December 2021.

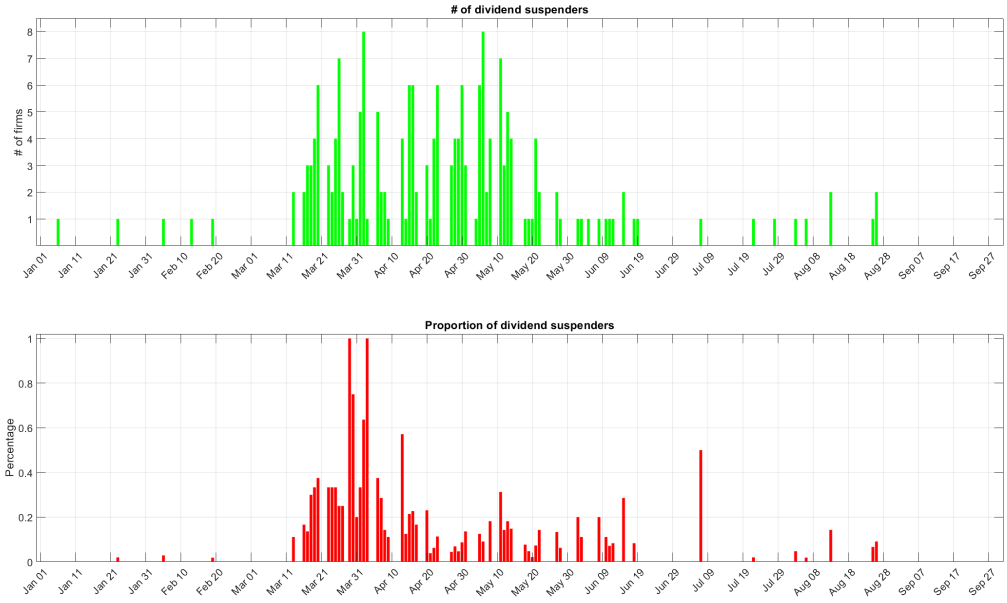

Figure 1. Distribution of dividend suspenders during the period from January 1st to September 30st 2020. This figure plots time series of daily dividend suspensions since the start of 2020. For each day, the top panel shows the number of firms which announce a dividend suspension, while the bottom panel shows the total market capitalization of the dividend suspenders on those same days.

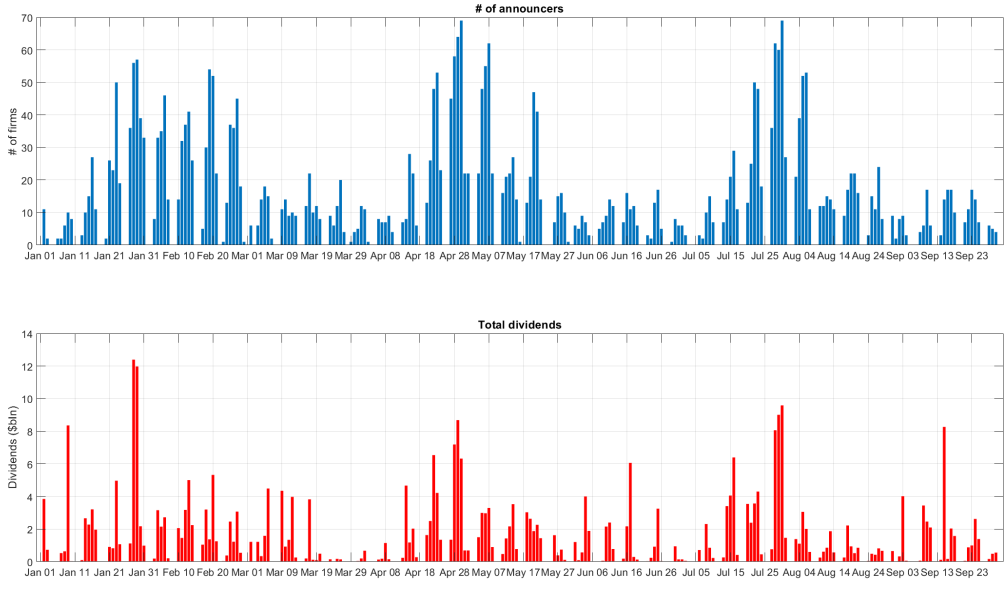

Figure 2. Distribution of dividend announcements during the period from January 1st to September 30st 2020. This figure plots time series of dividend announcements since the start of 2020. For each day , the top panel shows the number of firms announcing dividends (both positive and suspenders). The bottom panel shows the overall nominal amount of dividends announced by those firms (in billion dollars).

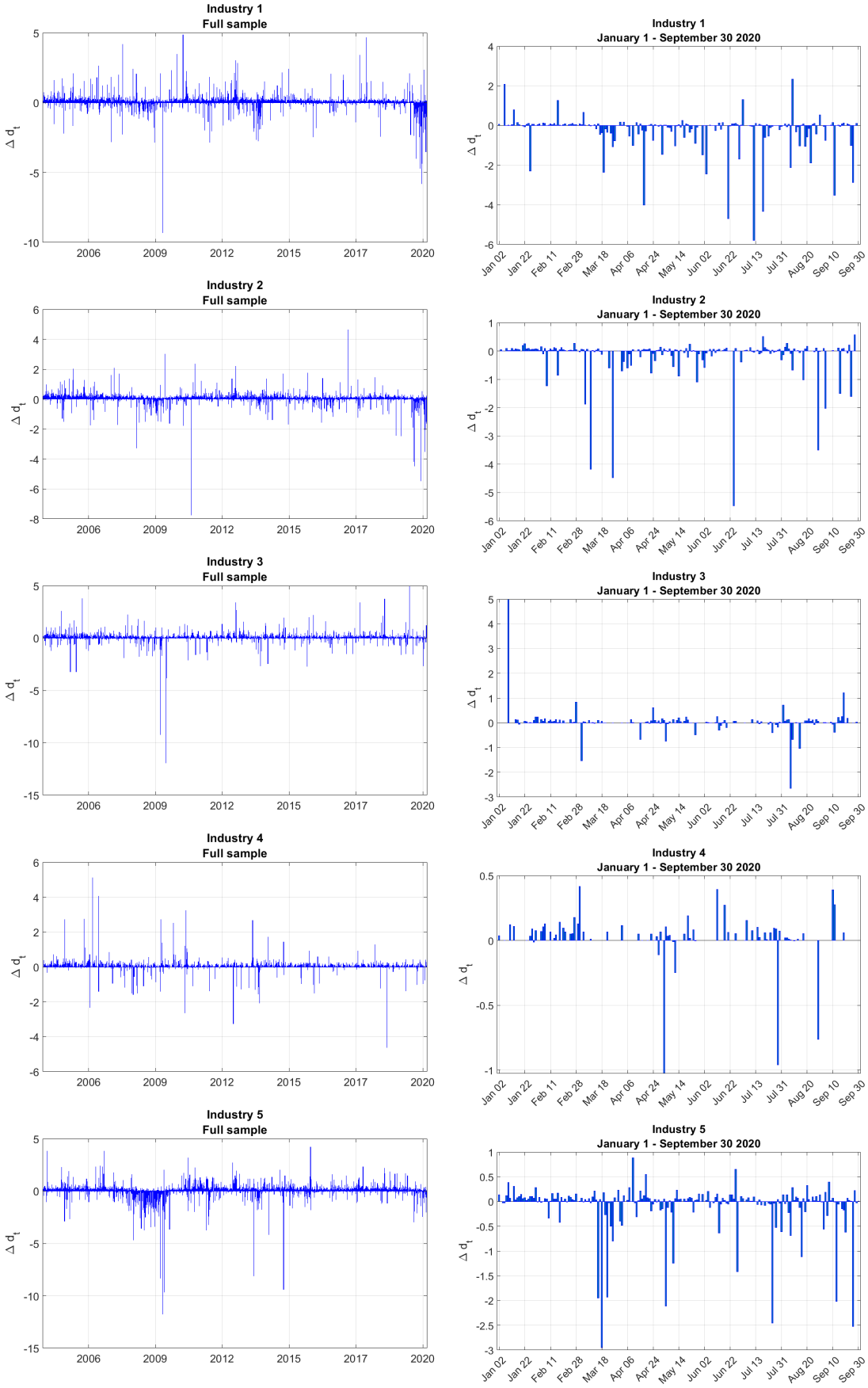

Figure 3: Daily dividend growth during the full sample and the 2020 sub-sample. The left panels of this figure show the daily dividend growth series Δd_t^i for the five different industries over the full sample, January 2005–September 2020, while the right panels zoom into the 2020 subsample. Each row shows the dividend growth series for a different industry.

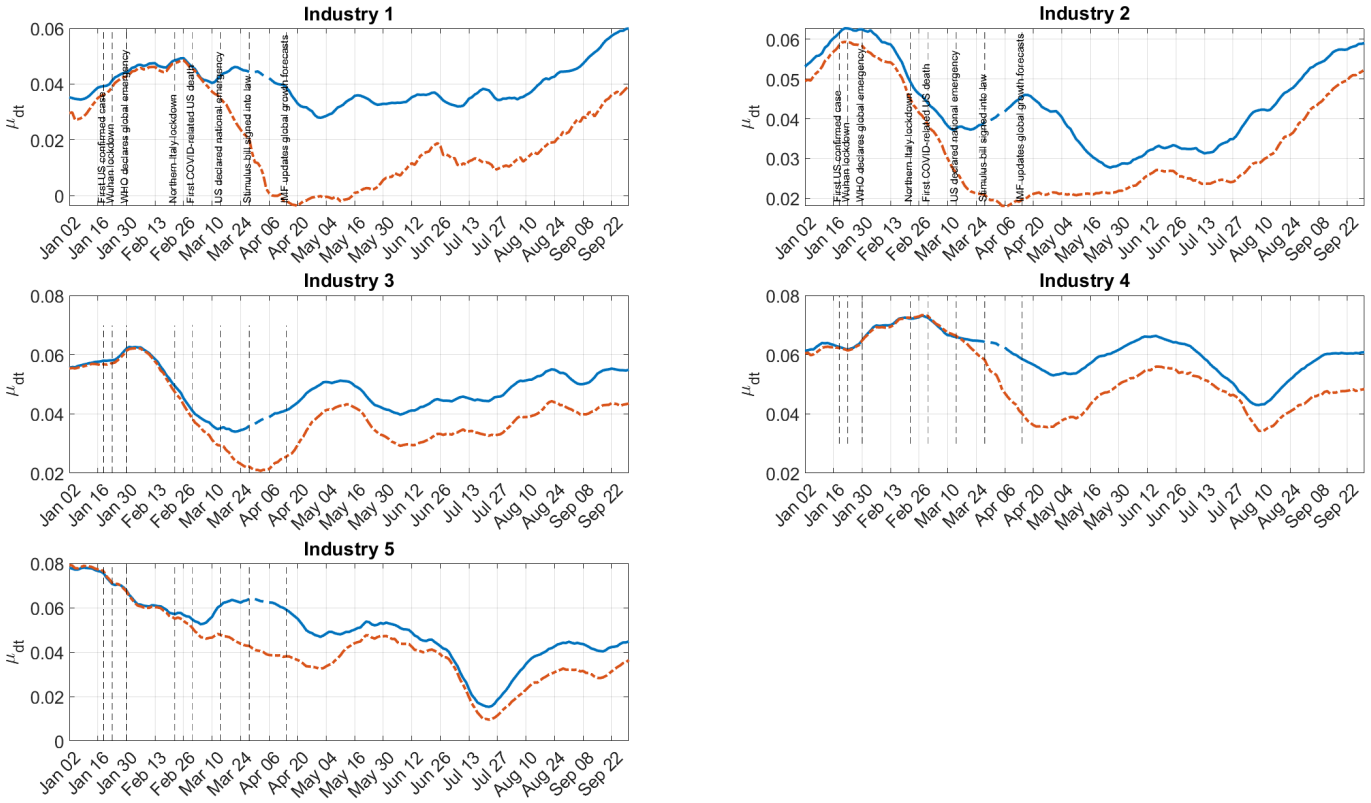

Figure 4: Comparison between our daily μ^i_{dt} with and without dividend suspenders. This figure plots our daily μ^i_{dt} with and without dividend suspenders. In both panels, the blue line shows the persistent component in dividend growth without taking into account dividend suspenders, while the red dotted line incorporates the information coming from the announcement of dividend suspenders, both in the construction of Δd^i_t and in accounting for the suspenders' dynamics in the econometric model.

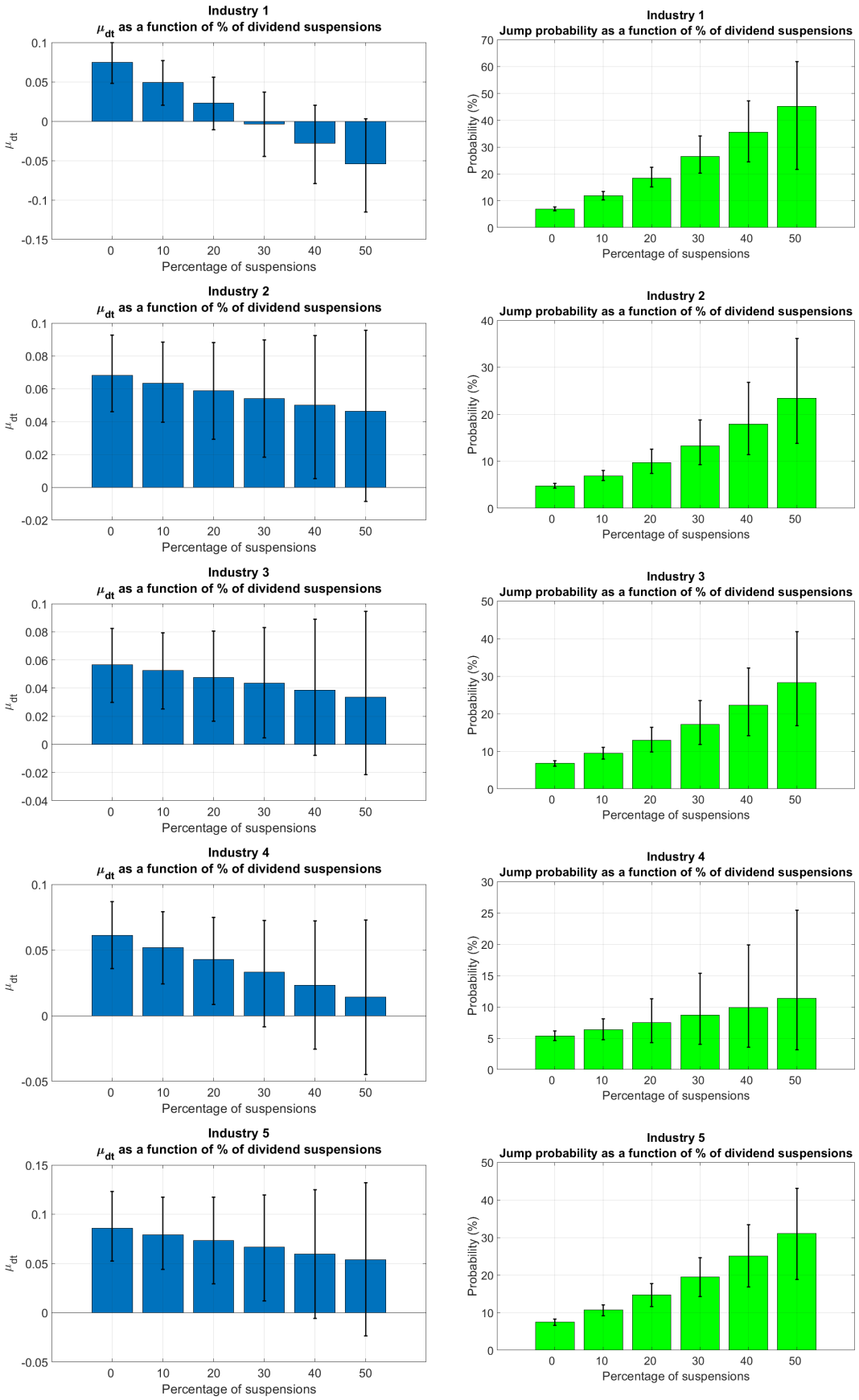

Figure 5: μ^i_{dt} and jump probability as a function of the fraction of dividend suspenders. This figure plots μ^i_{dt} (left panels) and the jump probability (right panels) as a function of the proportion of dividend suspensions, $N_{st+1}/\left(N_{dt+1}+N_{st+1}\right)$, fixing the number of announcers N_{st+1} at its historical average. Each row shows a different industry.

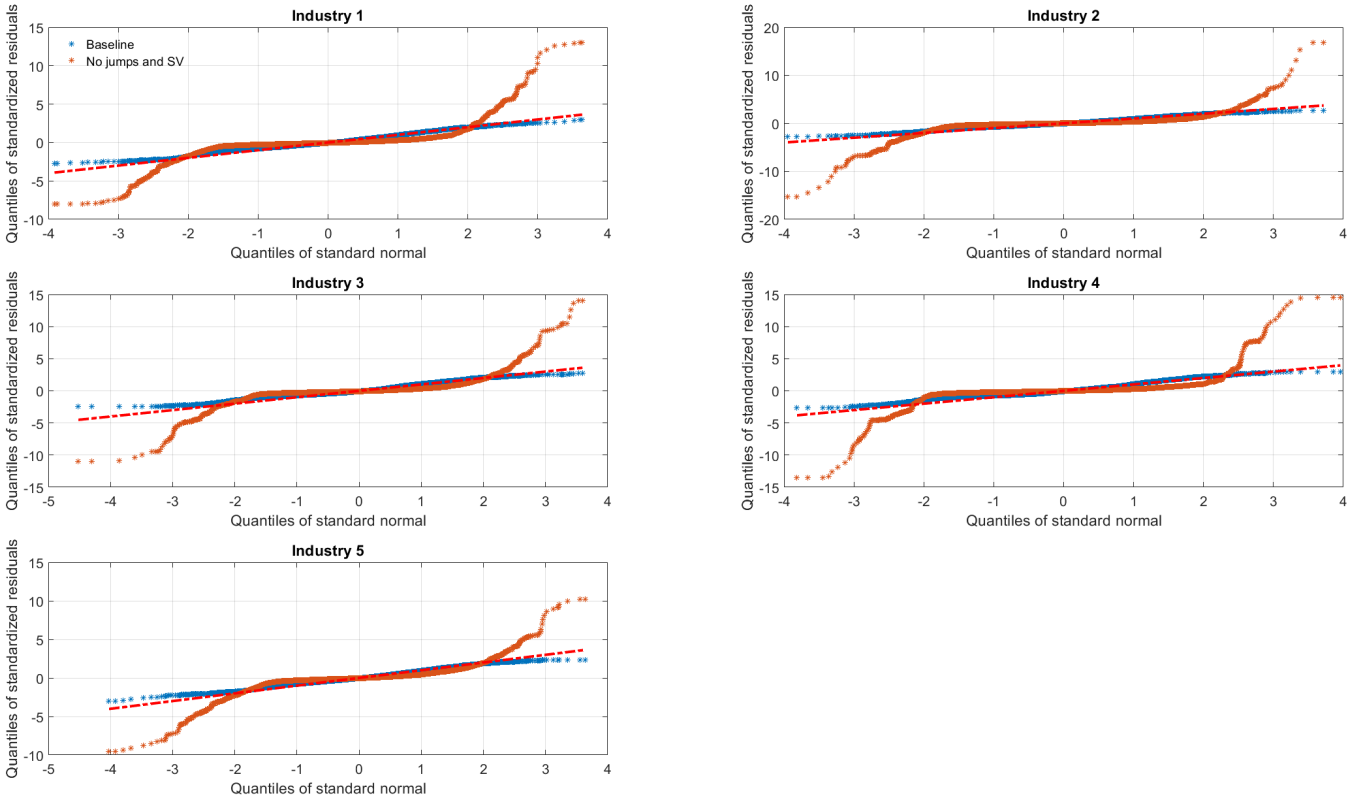

Figure 6: QQ-plots of standardized residuals, all industries. Each panel of this figure shows the Quantile-Quantile plot of the standardized residuals of the model described in Section 3 (in blue) as well as a variant of that same model estimated without jumps and SV (in brown), plotted against the 45 degree line (shown in red).

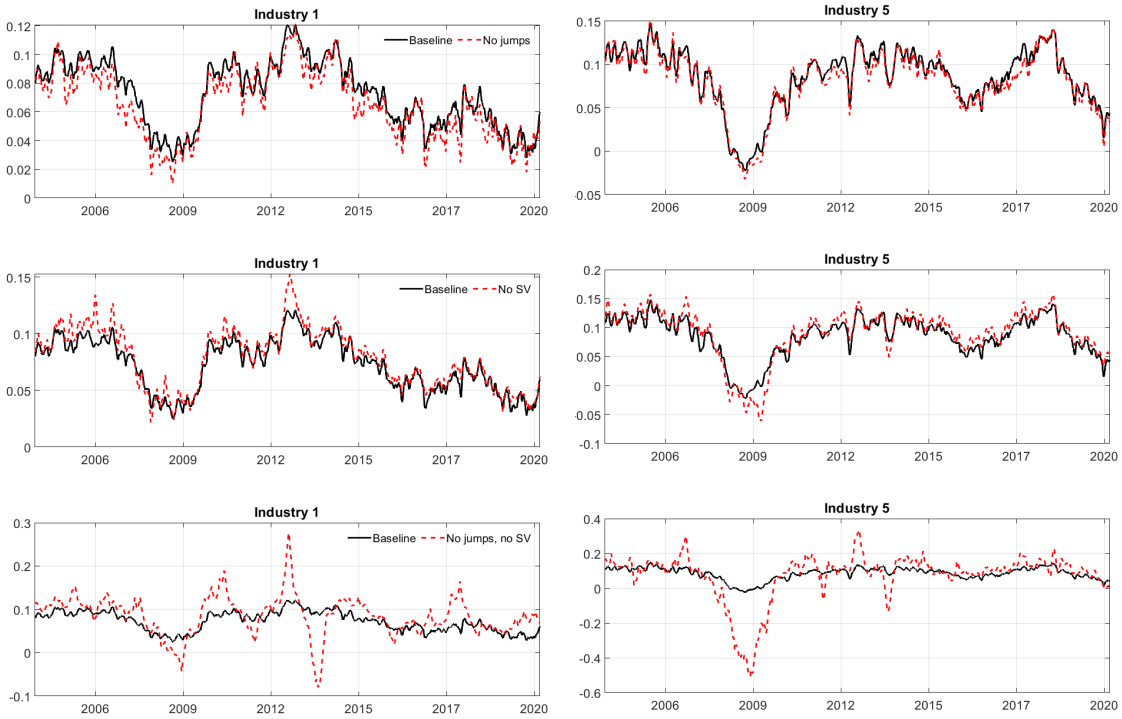

Figure 7: Model specification analysis - μ^i_{dt}**.** The top two panels show the times series of the latent μ^i_{dt} component estimated either using the baseline model (in black) or a model without jumps, for industries one (left panel) and five (right panel). The middle and bottom panels repeat the same experiment, where in the middle panels we are plotting the μ^i_{dt} component for the baseline model (in black) against a model without SV, while in the bottom panels we are plotting the μ^i_{dt} component for the baseline model (in black) against a model with neither jumps or SV.

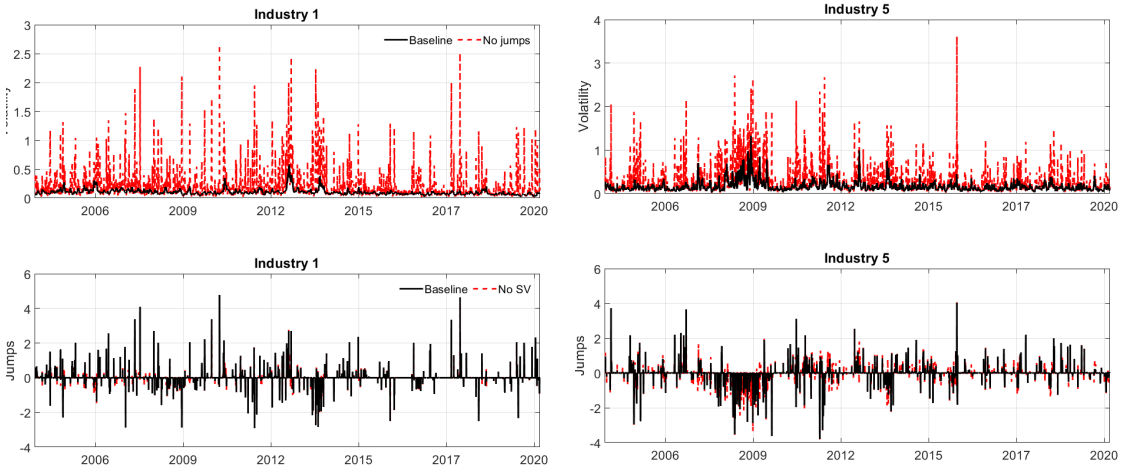

Figure 8: Model specification analysis - $\exp(h^i_{dt}/2)$ **and** $J^i_{dt}\xi^i_{dt}$**.** The top panel shows the time series of the latent volatility $\exp(h^i_{dt}/2)$ component estimated either using the baseline model (in black) or a model without jumps, for industries one (left panel) and five (right panel). The bottom panel repeats the same analysis by plotting the time series of estimated jumps in the dividend growth series, $J^i_{dt}\xi^i_{dt}$, for the baseline model (in black) and a model without SV.

Figure 9: Stochastic volatility of the daily dividend growth series against VIX and futures returns volatility. This figure plots the stochastic volatility of the daily dividend growth series - with dividend suspenders - against the daily VIX, the Economic Policy Uncertainty index (left) and the time-varying volatility of two different dividend futures returns, extracted using a GARCH(1,1) model (right). Each row shows results for a different industry. The sample period is January 1, 2020 through September 30, 2020.

Appendix A MCMC Sampler

In this section we describe all steps in the MCMC sampler. We begin by rewriting the model in its most general form. We next turn to the posterior derivations for all latent states and model parameters.

A.1 Model

Let Δd_{t+1}^i denote the year on year dividend growth in industry i, with $i = 1, ..., K$. We combine all the industry growth rates into the vector $\Delta \boldsymbol{d}_{t+1} = \left(\Delta d_{t+1}^1, ..., \Delta d_{t+1}^K\right)'$ and specify the following model:[18]

$$\Delta \boldsymbol{d}_{t+1} = \boldsymbol{\mu}_{dt+1} + \boldsymbol{\xi}_{dt+1} \odot \boldsymbol{J}_{dt+1} + \boldsymbol{\Sigma}_{dt+1}^{1/2} \boldsymbol{\varepsilon}_{dt+1}, \tag{A.1}$$

where $\boldsymbol{\mu}_{dt+1} = \left(\mu_{dt+1}^1, ..., \mu_{dt+1}^K\right)'$, $\boldsymbol{\xi}_{dt+1} = \left(\xi_{dt+1}^1, ..., \xi_{dt+1}^K\right)'$, $\boldsymbol{J}_{dt+1} = \left(J_{dt+1}^1, ..., J_{dt+1}^K\right)'$ and $\boldsymbol{\varepsilon}_{dt+1} = \left(\varepsilon_{dt+1}^1, ..., \varepsilon_{dt+1}^K\right)' \sim \mathcal{N}\left(\boldsymbol{0}, \boldsymbol{I}_K\right)$ with $\boldsymbol{\Sigma}_{dt+1}$ a $K \times K$ diagonal matrix.

The vector of time-varying means $\boldsymbol{\mu}_{dt+1}$ follows a VAR-X(1),

$$\boldsymbol{\mu}_{dt+1} = \boldsymbol{\mu}_\mu + \boldsymbol{\Phi}_\mu \left(\boldsymbol{\mu}_{dt} - \boldsymbol{\mu}_\mu\right) + \boldsymbol{X}_{t+1}^\mu \boldsymbol{B}_\mu + \boldsymbol{\Sigma}_\mu^{1/2} \boldsymbol{\varepsilon}_{\mu t+1}, \quad \boldsymbol{\varepsilon}_{\mu t+1} \sim \mathcal{N}\left(\boldsymbol{0}, \boldsymbol{I}_K\right) \tag{A.2}$$

where

$$\boldsymbol{X}_{t+1}^\mu = \begin{bmatrix} \left(\boldsymbol{x}_{1,t+1}^\mu\right)' & \boldsymbol{0}' & \boldsymbol{0}' & \dots & \boldsymbol{0}' \\ \boldsymbol{0}' & \left(\boldsymbol{x}_{2,t+1}^\mu\right)' & \boldsymbol{0}' & \dots & \boldsymbol{0}' \\ \vdots & \vdots & \vdots & \ddots & \vdots \\ \boldsymbol{0}' & \boldsymbol{0}' & \boldsymbol{0}' & \dots & \left(\boldsymbol{x}_{K,t+1}^\mu\right)' \end{bmatrix} \tag{A.3}$$

includes all industry-specific exogenous regressors and $\boldsymbol{B}_\mu = \left(\boldsymbol{\beta}_{1\mu}', ..., \boldsymbol{\beta}_{K\mu}'\right)'$ collects the associated coefficients.

As for the time-varying variance-covariance of the model, we write

[18] $\odot$ denotes the Hadamard product.

$\mathbf{\Sigma}_{dt+1} = diag\left(e^{h^1_{dt+1}}, ..., e^{h^K_{dt+1}}\right)$, with

$$h^i_{dt+1} = \mu_{ih} + \phi_{ih}\left(h^i_{dt} - \mu_{ih}\right) + \xi^i_{ht+1}J^i_{dt+1} + \boldsymbol{\beta}'_{ih}\boldsymbol{x}^h_{i,t+1} + \sigma_{ih}\varepsilon^i_{ht+1}, \quad i = 1, ..., K \tag{A.4}$$

and where $\varepsilon^i_{ht+1} \sim \mathcal{N}(0, 1)$ independent among each other and across time.

Moving on to the industry-specific jump components of the model, starting with the jump timings we specify ($i = 1, ..., K$)

$$Pr(J^i_{dt+1} = 1 \Big| \boldsymbol{x}^J_{i,t+1}) = \Phi(\boldsymbol{\lambda}'_i\boldsymbol{x}^J_{i,t+1}) \tag{A.5}$$

while for the jump intensities we write ($i = 1, ..., K$)

$$\xi^i_{dt+1} \Big| xi^i_{ht+1} \sim \mathcal{N}(\rho_{iJ}\xi^i_{ht+1}, \sigma^2_{\xi^i_d}) \tag{A.6}$$

and

$$\xi^i_{ht+1} \sim \mathcal{N}(0, \sigma^2_{\xi^i_h}). \tag{A.7}$$

with ξ^i_{dt+1} and ξ^i_{ht+1} independent of $\boldsymbol{\varepsilon}_{dt+1}$, $\boldsymbol{\varepsilon}_{\mu t+1}$ and ε^i_{ht+1} at all times. Finally, we assume throughout that $J^i_{d0} = J^i_{d1} = 0$ for all i and $\Delta\boldsymbol{d}_0 = \mathbf{0}$.

A.2 Posterior simulator

As we discussed in the main body of the paper, we can simulate from the joint posterior distribution using the following sampler that sequentially draws from:

1. $\boldsymbol{\mu}_d \big| \boldsymbol{h}_d, \boldsymbol{\xi}_d, \boldsymbol{J}_d, \mathbf{\Theta}, \mathcal{D}^T$;
2. $\boldsymbol{h}^i_d \Big| \boldsymbol{\mu}^i_d, \boldsymbol{\xi}^i_d, \boldsymbol{\xi}^i_h, \boldsymbol{J}^i_d, \mathbf{\Theta}, \mathcal{D}^T$ ($i = 1, ..., K$);
3. $\boldsymbol{J}^i_d \Big| \boldsymbol{\mu}^i_d, \boldsymbol{\xi}^i_d, \boldsymbol{\xi}^i_h, \boldsymbol{h}^i_d, \mathbf{\Theta}, \mathcal{D}^T$ ($i = 1, ..., K$);
4. $\boldsymbol{\xi}^i_d \Big| \boldsymbol{\mu}^i_d, \boldsymbol{J}^i_d, \boldsymbol{\xi}^i_h, \boldsymbol{h}^i_d, \mathbf{\Theta}, \mathcal{D}^T$ ($i = 1, ..., K$);
5. $\boldsymbol{\xi}^i_h \Big| \boldsymbol{J}^i_d, \boldsymbol{h}^i_d, \mathbf{\Theta}, \mathcal{D}^T$ ($i = 1, ..., K$);

6. $\boldsymbol{\Theta} | \, \boldsymbol{\mu}_d, \boldsymbol{h}_d, \boldsymbol{\xi}_d, \boldsymbol{\xi}_h, \boldsymbol{J}_d, \mathcal{D}^T$.

We have already reviewed the first block as well the first three parts of the last block, so here we focus on blocks 2 to 5 as well the remaining steps of block 6.

A.2.1 $h_d^i \Big| \, \boldsymbol{\mu}_d^i, \boldsymbol{\xi}_d^i, \boldsymbol{\xi}_h^i, \boldsymbol{J}_d^i, \boldsymbol{\Theta}\mathcal{D}^T$ $(i = 1, ..., K)$

Start by combining the state equation for h_{dt+1}^i in (A.4) and the initial condition for h_{d1}^i in (10) to get

$$\boldsymbol{H}_{ih} \boldsymbol{h}_d^i = \widetilde{\boldsymbol{\delta}}_{ih} + \boldsymbol{\Sigma}_{ih}^{1/2} \boldsymbol{\varepsilon}_{ih}, \quad \boldsymbol{\varepsilon}_{ih} \sim \mathcal{N}(\boldsymbol{0}, \boldsymbol{I}_{TK}), \tag{A.8}$$

where

$$\boldsymbol{H}_{ih} = \begin{bmatrix} 1 & 0 & \dots & \dots & \dots & 0 \\ -\phi_{ih} & 1 & 0 & \dots & \dots & 0 \\ \vdots & \vdots & \vdots & \ddots & \vdots & \vdots \\ 0 & \dots & \dots & 0 & -\phi_{ih} & 1 \end{bmatrix}, \quad \widetilde{\boldsymbol{\delta}}_{ih} = \begin{bmatrix} \mu_{ih} + (1 - \phi_{ih})^{-1} \boldsymbol{\beta}_{ih}' \boldsymbol{x}_{i1}^h \\ (1 - \phi_{ih}) \mu_{ih} + \boldsymbol{\beta}_{ih}' \boldsymbol{x}_{i2}^h + \xi_{h2}^i J_{d2}^i \\ \dots \\ (1 - \phi_{ih}) \mu_{ih} + \boldsymbol{\beta}_{ih}' \boldsymbol{x}_{iT}^h + \xi_{hT}^i J_{dT}^i \end{bmatrix}, \tag{A.9}$$

$$\boldsymbol{\varepsilon}_{ih} = \begin{bmatrix} \varepsilon_{h1}^i \\ \varepsilon_{h2}^i \\ \dots \\ \varepsilon_{hT}^i \end{bmatrix}, \text{and} \quad \boldsymbol{\Sigma}_{ih} = \begin{bmatrix} \frac{\sigma_{ih}^2}{(1 - \phi_{ih}^2)} & & & \\ & \sigma_{ih}^2 & & \\ & & \ddots & \\ & & & \sigma_{ih}^2 \end{bmatrix}. \tag{A.10}$$

This leads to

$$\boldsymbol{h}_d^i \sim \mathcal{N}\left(\boldsymbol{\delta}_{ih}, \left(\boldsymbol{H}_{ih}' \boldsymbol{\Sigma}_{ih}^{-1} \boldsymbol{H}_{ih} \right)^{-1} \right), \tag{A.11}$$

where $\boldsymbol{\delta}_{ih} = \boldsymbol{H}_{ih}^{-1} \widetilde{\boldsymbol{\delta}}_{ih}$. Next, note that the observation equation is a nonlinear function of $\boldsymbol{h}_d^i$, so we first rewrite it as

$$\log\left(\Delta d_t^{i,\star\star} \right)^2 = h_{dt}^i + \log\left(\varepsilon_{dt}^i \right)^2, \quad t = 1, ..., T, \tag{A.12}$$

where $\Delta d_t^{i,\star\star} = \Delta d_t^i - \mu_{dt}^i - \xi_{dt}^i J_{dt}^i$. We follow Kim, Shephard, and Chib (1998) and approximate $\log\left(\varepsilon_{dt}^i\right)^2$ with a mixture of normal distributions,

$$\log\left(\varepsilon_{dt}^i\right)^2 \approx \sum_{j=1}^{7} q_j \times \mathcal{N}\left(m_j - 1.2704, v_j^2\right), \tag{A.13}$$

where m_j, v_j^2, and q_j are constants specified in Kim et al. (1998). Along with (A.13), we also introduce a vector of state variables $\boldsymbol{s}_d^i = \left\{s_{dt}^i\right\}_{t=1}^T$ such that $\Pr\left(s_{dt}^i = j\right) = q_j$, for $j = 1, .., 7$ and $t = 1, ..., T$. Conditional on a particular realization of this vector of state variables, we can rewrite the observation equation in (A.12) in compact form as

$$\log\left(\Delta \boldsymbol{d}^{i,\star\star}\right)^2 \Big| \boldsymbol{\mu}_d^i, \boldsymbol{h}_d^i, \boldsymbol{J}_d^i, \boldsymbol{\xi}_d^i, \boldsymbol{s}_d^i \sim \mathcal{N}(\boldsymbol{m}_i + \boldsymbol{h}_d^i, \boldsymbol{V}_i), \tag{A.14}$$

where

$$\boldsymbol{m}_i = \begin{bmatrix} m_{s_{d1}^i} - 1.2704 \\ m_{s_{d2}^i} - 1.2704 \\ \vdots \\ m_{s_{dT}^i} - 1.2704 \end{bmatrix}, \quad \boldsymbol{V}_i = \begin{bmatrix} v^2_{s_{d1}^i} & & & \\ & v^2_{s_{d2}^i} & & \\ & & \ddots & \\ & & & v^2_{s_{dT}^i} \end{bmatrix}. \tag{A.15}$$

Combining (A.14) and (A.11) leads to the following posterior for $\boldsymbol{h}_d^i$

$$\boldsymbol{h}_d^i \Big| \boldsymbol{\mu}_d^i, \boldsymbol{\xi}_d^i, \boldsymbol{\xi}_h^i, \boldsymbol{J}_d^i, \boldsymbol{\Theta}, \mathcal{D}^T \sim \mathcal{N}\left(\boldsymbol{K}_{ih}^{-1}\boldsymbol{k}_{ih}, \boldsymbol{K}_{ih}^{-1}\right), \tag{A.16}$$

where

$$\boldsymbol{K}_{ih} = \boldsymbol{H}_{ih}'\boldsymbol{\Sigma}_{ih}^{-1}\boldsymbol{H}_{ih} + \boldsymbol{V}_i \tag{A.17}$$

$$\boldsymbol{k}_{ih} = \boldsymbol{H}_{ih}'\boldsymbol{\Sigma}_{ih}^{-1}\boldsymbol{H}_{ih}\boldsymbol{\delta}_{ih} + \boldsymbol{V}_i^{-1}\left(\log\left(\Delta \boldsymbol{d}^{i,\star\star}\right)^2 - \boldsymbol{m}_i\right). \tag{A.18}$$

As for drawing the vector of state variables s_d^i, note that

$$\Pr\left(s_{dt}^i = j \middle| \mu_{dt}^i, \xi_{dt}^i, J_{dt}^i, h_{dt}^i, \boldsymbol{\Theta}, \mathcal{D}^T\right) = \frac{q_j \times f_{\mathcal{N}}\left(\log\left(\Delta d_t^{i,**}\right)^2 \middle| h_{dt}^i + m_j - 1.2704, v_j^2\right)}{\sum_{l=1}^7 q_l \times f_{\mathcal{N}}\left(\log\left(\Delta d_t^{i,**}\right)^2 \middle| h_{dt}^i + m_l - 1.2704, v_l^2\right)},$$

where $j = 1, ..., 7$, $t = 1, ..., T$, and $f_{\mathcal{N}}(y|\, a, b)$ denotes the kernel of a normal distribution with mean a and variance b evaluated at y.

A.2.2 $\boldsymbol{J}_d^i \middle| \boldsymbol{\mu}_d^i, \boldsymbol{\xi}_d^i, \boldsymbol{\xi}_h^i, \boldsymbol{h}_d^i, \boldsymbol{\Theta}, \mathcal{D}^T$ $(i = 1, ..., K)$

Note that for any given $t \in [2, T]$

$$\begin{aligned}\Pr\left(J_{dt}^i = 1 \middle| \mu_{dt}^i, \xi_{dt}^i, \xi_{ht}^i, h_{dt}^i, \boldsymbol{\Theta}, \mathcal{D}^T\right) \propto & p(\Delta d_t^i, h_{dt}^i \middle| \mu_{dt}^i, \xi_{dt}^i, \xi_{ht}^i, J_{dt}^i = 1, \boldsymbol{x}_{it}^h, \boldsymbol{\Theta}) \\ & \times \Pr(J_{dt}^i = 1 | \boldsymbol{x}_{it}^J, \boldsymbol{\Theta})\end{aligned} \tag{A.19}$$

where

$$p(\Delta d_t^i, h_{dt}^i \middle| \mu_{dt}^i, \xi_{dt}^i, \xi_{ht}^i, J_{dt}^i = 1, \boldsymbol{x}_{it}^h, \boldsymbol{\Theta}) \sim \mathcal{MVN}\left(\begin{bmatrix}\Delta d_t^i \\ h_{dt}^i\end{bmatrix} \middle| \begin{bmatrix}\mu_{dt}^i + \xi_{dt}^i \\ \mu_{ih} + \phi_{ih}(h_{dt-1}^i - \mu_{ih}) + \xi_{ht}^i + \boldsymbol{\beta}_{ih}' \boldsymbol{x}_{it}^h\end{bmatrix}, \begin{bmatrix}e^{h_{dt}^i} & 0 \\ 0 & \sigma_{ih}^2\end{bmatrix}\right)$$

and $\Pr\left(J_{dt}^i = 1 | \boldsymbol{x}_{it}^J, \boldsymbol{\Theta}\right) = \Phi\left(\boldsymbol{\lambda}_i' \boldsymbol{x}_{it}^J\right)$ while

$$p(\Delta d_t^i, h_{dt}^i \middle| \mu_{dt}^i, \xi_{dt}^i, \xi_{ht}^i, J_{dt}^i = 0, \boldsymbol{x}_{it}^h, \boldsymbol{\Theta}) \sim \mathcal{MVN}\left(\begin{bmatrix}\Delta d_t^i \\ h_{dt}^i\end{bmatrix} \middle| \begin{bmatrix}\mu_{dt}^i \\ \mu_{ih} + \phi_{ih}(h_{dt-1}^i - \mu_{ih}) + \boldsymbol{\beta}_{ih}' \boldsymbol{x}_{it}^h\end{bmatrix}, \begin{bmatrix}e^{h_{dt}^i} & 0 \\ 0 & \sigma_{ih}^2\end{bmatrix}\right)$$

and $\Pr\left(J_{dt}^i = 0 \middle| \boldsymbol{x}_{it}^J, \boldsymbol{\Theta}\right) = 1 - \Phi\left(\boldsymbol{\lambda}_i' \boldsymbol{x}_{it}^J\right)$.

A.3 $\boldsymbol{\xi}_d^i \Big| \boldsymbol{\mu}_d^i, \boldsymbol{J}_d^i, \boldsymbol{\xi}_h^i, \boldsymbol{h}_d^i, \boldsymbol{\Theta}, \mathcal{D}^T$ $(i = 1, ..., K)$

Start by noting that for any given $t \in [2, T]$, when $J_{dt}^i = 0$,

$$\xi_{dt}^i \Big| \boldsymbol{\mu}_d^i, \boldsymbol{J}_d^i, \boldsymbol{\xi}_h^i, \boldsymbol{h}_d^i, \boldsymbol{\Theta}, \mathcal{D}^T \sim \mathcal{N}(\rho_{iJ}\xi_{ht}^i, \sigma^2_{\xi_d^i}) \tag{A.20}$$

In other words, when $J_{dt}^i = 0$ we rely on ξ_{dt}^i prior distribution in (A.6). In contrast, when $J_{dt}^i = 1$, it is possible to rewrite the i-th row of the model in (A.1) as

$$\Delta d_t^i - \mu_{dt}^i = \xi_{dt}^i + e^{h_{dt}^i/2}\varepsilon_{dt}^i, \quad \varepsilon_{dt}^i \sim \mathcal{N}(0, 1). \tag{A.21}$$

Combining (A.21) with (A.6) leads to:

$$\xi_{dt}^i \Big| \boldsymbol{\mu}_d^i, \boldsymbol{J}_d^i, \boldsymbol{\xi}_h^i, \boldsymbol{h}_d^i, \boldsymbol{\Theta}, \mathcal{D}^T \sim \mathcal{N}(\overline{\mu}_{\xi_{dt}^i}, \overline{\sigma}^2_{\xi_{dt}^i}) \tag{A.22}$$

where

$$\begin{aligned} \overline{\sigma}^2_{\xi_{dt}^i} &= \left(\sigma^{-2}_{\xi_d^i} + e^{-h_{dt}^i}\right)^{-1} \\ \overline{\mu}_{\xi_{dt}^i} &= \overline{\sigma}^2_{\xi_{dt}^i}\left(\rho_{iJ}\xi_{ht}^i/\sigma^2_{\xi_d^i} + e^{-h_{dt}^i}\left(\Delta d_t^i - \mu_{dt}^i\right)\right). \end{aligned} \tag{A.23}$$

A.4 $\boldsymbol{\xi}_h^i \Big| \boldsymbol{J}_d^i, \boldsymbol{h}_d^i, \boldsymbol{\Theta}, \mathcal{D}^T$ $(i = 1, ..., K)$

Again, start by noting that when $J_{dt}^i = 0$, $\xi_{ht}^i \big| \mathcal{D}^T \sim \mathcal{N}(0, \sigma^2_{\xi_h^i})$. That is, when $J_{dt}^i = 0$ we rely on ξ_{ht}^i's prior distribution in (A.7). In contrast, when $J_{dt}^i = 1$, it is possible to rewrite the state equation for h_{dt}^i in (A.4) (for $t \in [2, T]$) as

$$h_{dt}^i - \mu_{ih} - \phi_{ih}\left(h_{dt-1}^i - \mu_{ih}\right) - \boldsymbol{\beta}_{ih}'\boldsymbol{x}_{it}^h = \xi_{ht}^i + \sigma_{ih}\varepsilon_{ht}^i, \quad \varepsilon_{ht}^i \sim \mathcal{N}(0, 1). \tag{A.24}$$

Combining (A.24) with (A.7) leads to:

$$\xi_{ht}^i \Big| J_{dt}^i = 1, h_{dt}^i, \boldsymbol{\Theta}, \mathcal{D}^T \sim \mathcal{N}(\overline{\mu}_{\xi_{ht}^i}, \overline{\sigma}^2_{\xi_{ht}^i}) \tag{A.25}$$

where

$$\begin{aligned}\overline{\sigma}^2_{\xi^i_{ht}} &= \left(\sigma^{-2}_{\xi^i_h} + \sigma^{-2}_{ih}\right)^{-1} \\ \overline{\mu}_{\xi^i_{ht}} &= \overline{\sigma}^2_{\xi^i_{ht}} \left(\sigma^{-2}_{ih}\left(h^i_{dt} - \mu_{ih} - \phi_{ih}\left(h^i_{dt-1} - \mu_{ih}\right) - \boldsymbol{\beta}'_{ih}\boldsymbol{x}^h_{it}\right)\right).\end{aligned} \tag{A.26}$$

A.5 $\boldsymbol{\Theta}|\,\boldsymbol{\mu}_d, \boldsymbol{h}_d, \boldsymbol{\xi}_d, \boldsymbol{\xi}_h, \boldsymbol{J}_d, \mathcal{D}^T$

We break the posterior into 12 separate parts and focus on blocks 4 to 12:[19]

- $\boldsymbol{B}_\mu|\boldsymbol{\mu}_d, \boldsymbol{\Theta}_{-\boldsymbol{B}_\mu}, \mathcal{D}^T$:

  Start by rewriting (A.2) as follows

$$\boldsymbol{Z}_{B_\mu} = \boldsymbol{W}_{B_\mu}\boldsymbol{B}_\mu + \boldsymbol{\Omega}_\mu^{1/2}\boldsymbol{\varepsilon}_\mu \quad \boldsymbol{\varepsilon}_\mu \sim \mathcal{N}(\boldsymbol{0}, \boldsymbol{I}_{TK}) \tag{A.27}$$

  where

$$\boldsymbol{Z}_{B_\mu} = \begin{bmatrix} \boldsymbol{\mu}_{d1} - \boldsymbol{\mu}_d \\ \boldsymbol{\mu}_{d2} - \boldsymbol{\mu}_d - \boldsymbol{\Phi}_\mu(\boldsymbol{\mu}_{d1} - \boldsymbol{\mu}_d) \\ \vdots \\ \boldsymbol{\mu}_{dT} - \boldsymbol{\mu}_d - \boldsymbol{\Phi}_\mu(\boldsymbol{\mu}_{dT-1} - \boldsymbol{\mu}_d) \end{bmatrix}, \quad \boldsymbol{W}_{B_\mu} = \begin{bmatrix} (\boldsymbol{I}_K - \boldsymbol{\Phi}_\mu)^{-1}\boldsymbol{X}^\mu_1 \\ \boldsymbol{X}^\mu_2 \\ \vdots \\ \boldsymbol{X}^\mu_T \end{bmatrix}. \tag{A.28}$$

  Combing (A.27) with the prior for $\boldsymbol{\beta}_\mu$ in (14) after first defining $\underline{\boldsymbol{B}}_{\mu 0} = \left(\underline{\boldsymbol{\beta}}'_{\mu_0}, ..., \underline{\boldsymbol{\beta}}'_{\mu_0}\right)'$ and $\underline{\boldsymbol{V}}_{\boldsymbol{B}_\mu} = diag\left(diag\left(\underline{\boldsymbol{V}}_{\beta_\mu}\right)', ..., diag\left(\underline{\boldsymbol{V}}_{\beta_\mu}\right)'\right)'$ leads to the following posterior distribution:

$$\boldsymbol{B}_\mu|\boldsymbol{\mu}_d, \boldsymbol{\Theta}_{-\boldsymbol{B}_\mu}, \mathcal{D}^T \sim \mathcal{N}(\overline{\boldsymbol{B}}_\mu, \overline{\boldsymbol{V}}_{B_\mu}) \tag{A.29}$$

  where

$$\overline{\boldsymbol{V}}_{B_\mu} = \left(\underline{\boldsymbol{V}}^{-1}_{B_\mu} + \boldsymbol{W}'_{B_\mu}\boldsymbol{\Omega}^{-1}_\mu\boldsymbol{W}_{B_\mu}\right)^{-1} \tag{A.30}$$

[19] We use standard set notation to define $\mathcal{A}_{-b} = \{x \in \mathcal{A} : x \neq b\}$.

and

$$\overline{\boldsymbol{B}}_{\mu} = \overline{\boldsymbol{V}}_{B_{\mu}} \left(\underline{\boldsymbol{V}}_{B_{\mu}}^{-1} \underline{\boldsymbol{B}}_{\mu_0} + \boldsymbol{W}_{B_{\mu}}' \boldsymbol{\Omega}_{\mu}^{-1} \boldsymbol{Z}_{B_{\mu}} \right). \tag{A.31}$$

- $\mu_{ih} | \boldsymbol{h}_d^i, \boldsymbol{J}_d^i, \boldsymbol{\xi}_h^i, \boldsymbol{\Theta}_{-\mu_{ih}}, \mathcal{D}^T$ $(i = 1, ..., K)$:

  Start by combining (A.4) and (10) into:

$$\boldsymbol{Z}_{\mu_{ih}} = \boldsymbol{W}_{\mu_{ih}} \mu_{ih} + \boldsymbol{\Sigma}_{ih}^{1/2} \boldsymbol{\varepsilon}_{ih} \quad \boldsymbol{\varepsilon}_{ih} \sim \mathcal{N}(\boldsymbol{0}, \boldsymbol{I}_T) \tag{A.32}$$

  where

$$\boldsymbol{W}_{\mu_{ih}} = \begin{bmatrix} 1 \\ 1 - \phi_{ih} \\ \vdots \\ 1 - \phi_{ih} \end{bmatrix}, \quad \boldsymbol{Z}_{\mu_{ih}} = \begin{bmatrix} h_{d1}^i - \frac{\boldsymbol{\beta}_{ih}' \boldsymbol{x}_{i1}^h}{1 - \phi_{ih}} \\ h_{d2}^i - \phi_{ih} h_{d1}^i - \boldsymbol{\beta}_{ih}' \boldsymbol{x}_{i2}^h - J_{d2}^i \xi_{h2}^i \\ \vdots \\ h_{dT}^i - \phi_{ih} h_{dT-1}^i - \boldsymbol{\beta}_{ih}' \boldsymbol{x}_{iT}^h - J_{dT}^i \xi_{hT}^i \end{bmatrix}. \tag{A.33}$$

  Next, combine (A.32) with the prior for μ_{ih} in (12) to get

$$\mu_{ih} | \boldsymbol{h}_d^i, \boldsymbol{J}_d^i, \boldsymbol{\xi}_h^i, \boldsymbol{\Theta}_{-\mu_{ih}}, \mathcal{D}^T \sim \mathcal{N} \left(\overline{\mu}_{ih}, \overline{V}_{\mu_{ih}} \right) \tag{A.34}$$

  where

$$\overline{V}_{\mu_{ih}} = \left[\underline{V}_{\mu_h}^{-1} + \boldsymbol{W}_{\mu_{ih}}' \boldsymbol{\Sigma}_{ih}^{-1} \boldsymbol{W}_{\mu_{ih}} \right]^{-1} \tag{A.35}$$

  and

$$\overline{\mu}_{ih} = \overline{V}_{\mu_{ih}} \left[\underline{V}_{\mu_h}^{-1} \underline{\mu}_{h0} + \boldsymbol{W}_{\mu_{ih}}' \boldsymbol{\Sigma}_{ih}^{-1} \boldsymbol{Z}_{\mu_{ih}} \right] \tag{A.36}$$

- $\phi_{ih} | \boldsymbol{h}_d^i, \boldsymbol{J}_d^i, \boldsymbol{\xi}_h^i, \boldsymbol{\Theta}_{-\phi_{ih}}, \mathcal{D}^T$ $(i = 1, ..., K)$:

  As with $\boldsymbol{\Phi}_{\mu}$, we follow Kim et al. (1998) and first obtain a candidate draw from the

following distribution:

$$\phi_{ih}^{\star} \sim \mathcal{N}\left(\overline{\phi}_{ih}, \overline{V}_{\phi_{ih}}\right) \times I\left(|\phi_{ih}| < 1\right) \tag{A.37}$$

where

$$\overline{V}_{\phi_{ih}} = \left(\underline{V}_{\phi_h}^{-1} + \frac{\boldsymbol{W}_{\phi_{ih}}' \boldsymbol{W}_{\phi_{ih}}}{\sigma_{ih}^2}\right)^{-1}, \tag{A.38}$$

$$\overline{\phi}_{ih} = \overline{V}_{\phi_{ih}} \left(\underline{V}_{\phi_h}^{-1} \underline{\phi}_{h_0} + \frac{\boldsymbol{W}_{\phi_{ih}}' \boldsymbol{Z}_{\phi_{ih}}}{\sigma_{ih}^2}\right) \tag{A.39}$$

and where

$$\boldsymbol{Z}_{\phi_{ih}} = \begin{bmatrix} h_{d2}^i - \mu_{ih} - \boldsymbol{\beta}_{ih}' \boldsymbol{x}_2^{ih} - J_{d2}^i \xi_{h2}^i \\ \vdots \\ h_{dT}^i - \mu_{ih} - \boldsymbol{\beta}_{ih}' \boldsymbol{x}_T^{ih} - J_{dT}^i \xi_{hT}^i \end{bmatrix}, \quad \boldsymbol{W}_{\phi_{ih}} = \begin{bmatrix} h_{d1}^i - \mu_{ih} \\ \vdots \\ h_{dT-1}^i - \mu_{ih} \end{bmatrix} \tag{A.40}$$

Next, if the draw is retained (i.e., satisfy the stationarity restriction), we accept ϕ_{ih}^* with probability $e^{\left(g\left(\phi_{ih}^*\right) - g\left(\phi_{ih}^{old}\right)\right)}$ where ϕ_{ih}^{old} is the retained draw from the previous iteration of the Gibbs sampler, and

$$g\left(\phi_{ih}\right) = \ln p\left(\phi_{ih}\right) - \frac{1}{2} \ln\left(\frac{\sigma_{ih}^2}{1 - \phi_{ih}^2}\right) - \frac{\left(1 - \phi_{ih}^2\right)}{2\sigma_{ih}^2} \left(h_{d1}^i - \mu_{ih} - \frac{\boldsymbol{\beta}_{ih}' \boldsymbol{x}_1^{ih}}{1 - \phi_{ih}}\right)^2 \tag{A.41}$$

with $p\left(\phi_{ih}\right)$ denoting the prior of ϕ_{ih}.

- $\sigma_{ih}^2 | \boldsymbol{h}_d^i, \boldsymbol{J}_d^i, \boldsymbol{\xi}_h^i, \boldsymbol{\Theta}_{-\sigma_{ih}^2}, \mathcal{D}^T$ $(i = 1, ..., K)$:

The posterior for σ_{ih}^2 is readily available, and is given by:

$$\sigma_{ih}^2 | \boldsymbol{h}_d^i, \boldsymbol{J}_d^i, \boldsymbol{\xi}_h^i, \boldsymbol{\Theta}_{-\sigma_{ih}}, \mathcal{D}^T \sim \mathcal{IG}\left(\underline{V}_{ih} + \frac{T}{2}, \overline{S}_{ih}\right) \tag{A.42}$$

where

$$\overline{S}_{ih} = \underline{S}_h + \frac{1}{2}\left[\left(1-\phi_{ih}^2\right)\left(h_{d1}^i - \mu_{ih} - \frac{\boldsymbol{\beta}_{ih}'\boldsymbol{x}_{i1}^h}{1-\phi_h}\right)^2 + \sum_{t=1}^{T-1}\left(h_{dt+1}^i - \mu_{ih} - \phi_{ih}\left(h_{dt}^i - \mu_{ih}\right) - \boldsymbol{\beta}_{ih}'\boldsymbol{x}_{it+1}^h - J_{dt+1}^i\xi_{ht+1}^i\right)^2\right] \tag{A.43}$$

- $\boldsymbol{\beta}_{ih}|\boldsymbol{h}_d^i, \boldsymbol{J}_d^i, \boldsymbol{\xi}_h^i, \boldsymbol{\Theta}_{-\boldsymbol{\beta}_{ih}}, \mathcal{D}^T$ $(i = 1, ..., K)$:

  Start by rewriting (A.4) as follows

$$\boldsymbol{Z}_{\beta_{ih}} = \boldsymbol{W}_{\beta_{ih}}\boldsymbol{\beta}_{ih} + \boldsymbol{\Sigma}_{ih}^{1/2}\boldsymbol{\varepsilon}_{ih} \quad \boldsymbol{\varepsilon}_{ih} \sim \mathcal{N}(\boldsymbol{0}, \boldsymbol{I}_T) \tag{A.44}$$

  where

$$\boldsymbol{Z}_{\beta_{ih}} = \begin{bmatrix} h_{d1}^i - \mu_{ih} \\ h_d^i - \mu_{ih} - \phi_{ih}(h_{d1}^i - \mu_{ih}) - J_{d2}^i\xi_{h2}^i \\ \vdots \\ h_{dT}^i - \mu_{ih} - \phi_{ih}(h_{dT-1}^i - \mu_{ih}) - J_{dT}^i\xi_{hT}^i \end{bmatrix}, \quad \boldsymbol{W}_{\beta_{ih}} = \begin{bmatrix} (1-\phi_{ih})^{-1}\left(\boldsymbol{x}_{i1}^h\right)' \\ \left(\boldsymbol{x}_{i2}^h\right)' \\ \vdots \\ \left(\boldsymbol{x}_{iT}^h\right)' \end{bmatrix}. \tag{A.45}$$

  Combing (A.44) with the prior for $\boldsymbol{\beta}_{ih}$ in (14) leads to the following posterior distribution:

$$\boldsymbol{\beta}_{ih}|\boldsymbol{h}_d^i, \boldsymbol{J}_d^i, \boldsymbol{\xi}_h^i, \boldsymbol{\Theta}_{-\boldsymbol{\beta}_{ih}}, \mathcal{D}^T \sim \mathcal{N}(\overline{\boldsymbol{\beta}}_{ih}, \overline{\boldsymbol{V}}_{\beta_{ih}}) \tag{A.46}$$

  where

$$\overline{\boldsymbol{V}}_{\beta_{ih}} = \left(\underline{\boldsymbol{V}}_{\beta_h}^{-1} + \boldsymbol{W}_{\beta_{ih}}'\boldsymbol{\Sigma}_{ih}^{-1}\boldsymbol{W}_{\beta_{ih}}\right)^{-1} \tag{A.47}$$

  and

$$\overline{\boldsymbol{\beta}}_{ih} = \overline{\boldsymbol{V}}_{\beta_{ih}}\left(\underline{\boldsymbol{V}}_{\beta_h}^{-1}\underline{\boldsymbol{\beta}}_{h_0} + \boldsymbol{W}_{\beta_{ih}}'\boldsymbol{\Sigma}_{ih}^{-1}\boldsymbol{Z}_{\beta_{ih}}\right). \tag{A.48}$$

- $\boldsymbol{\lambda}_i | \, \boldsymbol{W}^i, \mathcal{D}^T$ and $\boldsymbol{W}^i \Big| \, \boldsymbol{\lambda}_i, \boldsymbol{J}_d^i, \mathcal{D}^T$ $(i = 1, ..., K)$:

  We follow Albert and Chib (1993) and to simplify the computations introduce the auxiliary latent state variable W_t^i, $t = 1, ..., T$. We proceed by first rewriting the stochastic process of the jump intensity in (A.5) as

$$J_{dt+1}^i = \begin{cases} 1 & \text{if } W_{t+1}^i > 0 \\ 0 & \text{if } W_{t+1}^i \leq 0 \end{cases} \tag{A.49}$$

  where

$$W_{t+1}^i = \boldsymbol{\lambda}_i' \boldsymbol{x}_{it+1}^J + \epsilon_{Wt+1}^i, \quad \epsilon_{Wt+1}^i \sim \mathcal{N}(0, 1) \tag{A.50}$$

  or, more compactly,

$$\boldsymbol{W}^i = \boldsymbol{X}_i^J \boldsymbol{\lambda}_i + \boldsymbol{\epsilon}_W^i, \quad \boldsymbol{\epsilon}_W^i \sim \mathcal{N}(\boldsymbol{0}, \boldsymbol{I}_T) \tag{A.51}$$

  where

$$\boldsymbol{X}_i^J = \begin{bmatrix} \left(\boldsymbol{x}_{i1}^J\right)' \\ \vdots \\ \left(\boldsymbol{x}_{iT}^J\right)' \end{bmatrix}, \quad \boldsymbol{W}^i = \begin{bmatrix} W_1^i \\ \vdots \\ W_T^i \end{bmatrix}. \tag{A.52}$$

  The posterior of $\boldsymbol{\lambda}_i$ is readily available, and given by

$$\boldsymbol{\lambda}_i | \, \boldsymbol{W}^i, \mathcal{D}^T \sim \mathcal{N}\left(\overline{\boldsymbol{\mu}}_{\lambda_i}, \overline{\boldsymbol{V}}_{\lambda_i}\right) \tag{A.53}$$

  where

$$\overline{\boldsymbol{V}}_{\lambda_i} = \left[\underline{\boldsymbol{V}}_\lambda^{-1} + \boldsymbol{X}_i^{J\prime} \boldsymbol{X}_i^J\right]^{-1} \tag{A.54}$$

  and

$$\overline{\boldsymbol{\mu}}_{\lambda_i} = \overline{\boldsymbol{V}}_{\lambda_i} \left[\underline{\boldsymbol{V}}_\lambda^{-1} \underline{\boldsymbol{\mu}}_\lambda + \boldsymbol{X}_i^{J\prime} \boldsymbol{W}^i\right]. \tag{A.55}$$

As for the sequence of latent variables $\left\{W_t^i\right\}_{t=1}^T$, we have that

$$W_t^i \Big| \boldsymbol{\lambda}_i, J_{dt}^i, \mathcal{D}^T \sim \begin{cases} TN(\boldsymbol{\lambda}_i' \boldsymbol{x}_{it+1}^J, 1, 0, \infty) & \text{if } J_{dt}^i = 1 \\ TN(\boldsymbol{\lambda}_i' \boldsymbol{x}_{it+1}^J, 1, -\infty, 0) & \text{if } J_{dt}^i = 0 \end{cases} \tag{A.56}$$

where $TN(\mu, \sigma^2, lb, ub)$ denotes a truncated normal distribution with mean μ, variance σ^2, and lower and upper bound lb, ub.

- $\sigma^2_{\xi_d^i} | \boldsymbol{\xi}_d^i, \boldsymbol{\xi}_h^i, \boldsymbol{\Theta}_{-\sigma^2_{\xi_d^i}}, \mathcal{D}^T$ $(i = 1, ..., K)$:

  The posterior distribution for $\sigma^2_{\xi_d^i}$ is readily available, and given by

$$\sigma^2_{\xi_d^i} \Big| \boldsymbol{\xi}_d^i, \boldsymbol{\xi}_h^i, \boldsymbol{\Theta}_{-\sigma^2_{\xi_d^i}}, \mathcal{D}^T \sim \mathcal{IG}\left(\underline{V}_{\xi^d} + \frac{T}{2}, \overline{S}_{\xi_d^i}\right) \tag{A.57}$$

  where

$$\overline{S}_{\xi_d^i} = \underline{S}_{\xi^d} + \frac{1}{2} \sum_{t=1}^{T} \left(\xi_{dt}^i - \rho_{iJ} \xi_{ht}^i\right)^2. \tag{A.58}$$

- $\sigma^2_{\xi_h^i} | \boldsymbol{\xi}_h^i, \mathcal{D}^T$:

  The posterior distribution for $\sigma^2_{\xi_h^i}$ is readily available, and given by

$$\sigma^2_{\xi_h^i} \Big| \boldsymbol{\xi}_h^i, \mathcal{D}^T \sim \mathcal{IG}\left(\underline{V}_{\xi^h} + \frac{T}{2}, \overline{S}_{\xi_h^i}\right) \tag{A.59}$$

  where

$$\overline{S}_{\xi_h^i} = \underline{S}_{\xi^h} + \frac{1}{2} \sum_{t=1}^{T} \left(\xi_{ht}^i\right)^2. \tag{A.60}$$

- $\rho_{iJ} | \boldsymbol{\xi}_d^i, \boldsymbol{\xi}_h^i, \boldsymbol{\Theta}_{-\rho_{iJ}}, \mathcal{D}^T$ $(i = 1, ..., K)$:

Start by rewriting (A.6) as

$$\xi_{dt}^{i} = \xi_{ht}^{i}\rho_{iJ} + \sigma_{\xi_d^i}\varepsilon_{\rho t}^{i} \quad \varepsilon_{\rho t}^{i} \sim \mathcal{N}(0,1) \tag{A.61}$$

It follows that

$$\rho_{iJ}|\boldsymbol{\xi}_d^i, \boldsymbol{\xi}_h^i, \boldsymbol{\Theta}_{-\rho_{iJ}}, \mathcal{D}^T \sim \mathcal{N}\left(\overline{\rho}_i, \overline{V}_{\rho_i}\right) \times I\left(\left|\rho_{iJ} < 1\right|\right) \tag{A.62}$$

where

$$\overline{V}_{\rho_i} = \left[\underline{V}_{\rho} + \frac{1}{\sigma_{\xi_d^i}^2}\left(\boldsymbol{\xi}_h^i\right)'\boldsymbol{\xi}_h^i\right]^{-1} \tag{A.63}$$

and

$$\overline{\rho}_i = \overline{V}_{\rho_i}\left[\frac{1}{\sigma_{\xi_d^i}^2}\left(\boldsymbol{\xi}_h^i\right)'\boldsymbol{\xi}_d^i\right]. \tag{A.64}$$

Appendix B Tables and Figures

Parameter estimates								
	Without suspenders				**With suspenders**			
	Mean	*Std*	*90% Credible Set*		*Mean*	*Std*	*90% Credible Set*	
μ_d	0.078	0.020	0.053	0.104	0.084	0.014	0.067	0.103
ϕ_μ	0.997	0.002	0.994	0.999	0.996	0.002	0.993	0.998
β_μ					-0.005	0.001	-0.008	-0.003
σ_μ	0.003	0.000	0.002	0.003	0.003	0.000	0.002	0.003
μ_h	-5.024	0.118	-5.216	-4.833	-4.566	0.219	-4.912	-4.190
ϕ_h	0.899	0.008	0.886	0.913	0.895	0.008	0.881	0.908
β_{h1}					1.003	0.310	0.497	1.512
β_{h2}					-0.266	0.104	-0.444	-0.096
σ_h	0.719	0.047	0.643	0.794	0.823	0.080	0.711	0.976
σ_ξ	2.871	0.044	2.798	2.943	2.920	0.044	2.848	2.993
σ_{ξ^h}	0.690	0.088	0.555	0.850	0.756	0.122	0.583	0.970
λ_1	-1.323	0.064	-1.429	-1.219	-1.360	0.079	-1.487	-1.227
λ_2	-0.018	0.003	-0.023	-0.013	-0.016	0.003	-0.021	-0.010
λ_3					1.893	0.635	0.865	2.945
λ_4	0.117	0.158	-0.150	0.378	0.005	0.221	-0.357	0.363
λ_5	-0.098	0.158	-0.360	0.153	-0.276	0.404	-1.072	0.103
ρ_J	-0.002	0.092	-0.159	0.147	-0.012	0.085	-0.154	0.124

Table B.1: Parameter estimates for the dividend growth rate model. This table shows parameter estimates for a range of models fitted to the daily dividend growth series. The equations for the most general version of the components model, estimated on the market dividend growth series. Within each panel, the columns report the posterior mean, standard deviation and 90% credible sets for all parameter estimates.

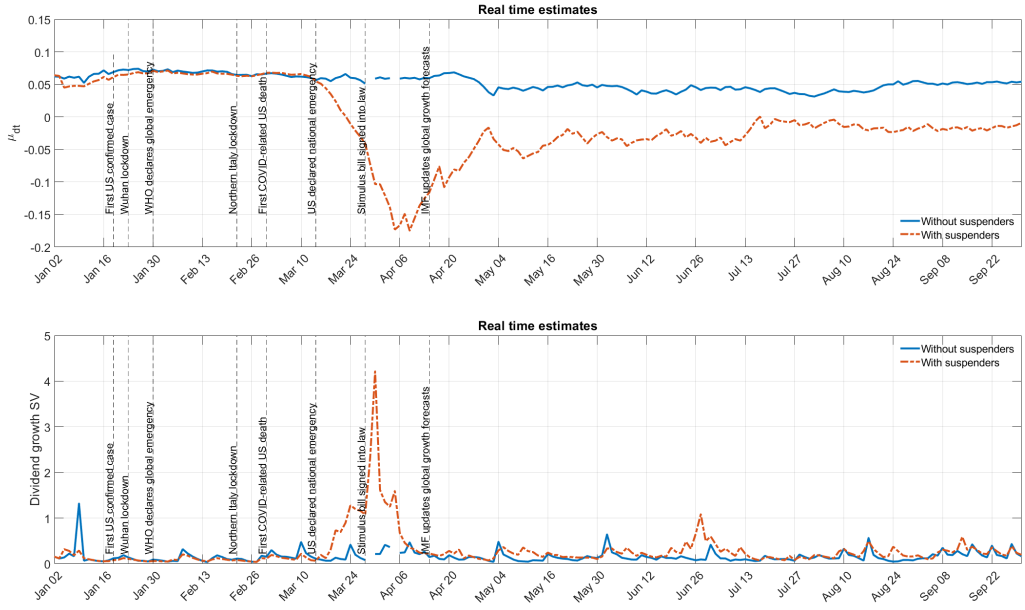

Figure B.1: Comparison between our daily μ_{dt} and $\exp(h_{dt}/2)$, with and without dividend suspenders, in real-time. The top panel plots the real-time versions of our daily μ_{dt} with and without dividend suspenders. The solid blue line shows the persistent component in dividend growth without taking into account dividend suspenders, while the red, dotted line incorporates the information coming from the announcement of dividend suspenders, both in the construction of Δd_t and in accounting for the suspenders' dynamics in the econometric model. The bottom figure plots the real-time versions of our daily $\exp(h_{dt}/2)$ with and without dividend suspenders. The solid blue line shows the stochastic volatility component without taking into account dividend suspenders, while the red, dotted line incorporates the information coming from the announcement of dividend suspenders, both in the construction of Δd_t and in accounting for the suspenders' dynamics in the econometric model.

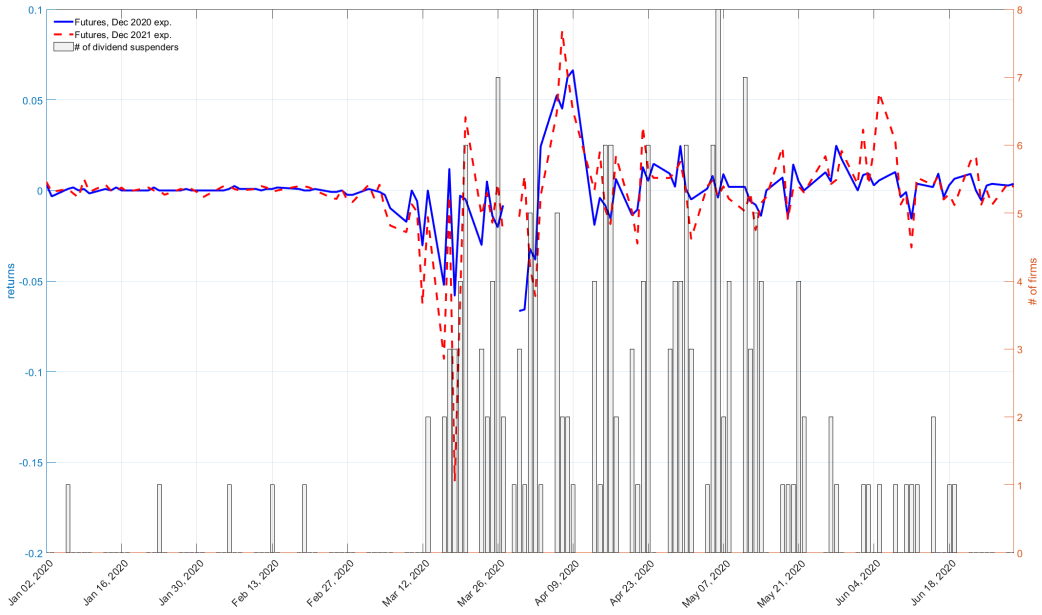

Figure B.2: Returns of dividend futures. This figure plots the returns of the dividend futures expiring in December 2020 and 2021 against the the total number of dividend suspenders over the period January-June 2020.